



저작자표시-비영리-변경금지 2.0 대한민국

이용자는 아래의 조건을 따르는 경우에 한하여 자유롭게

- 이 저작물을 복제, 배포, 전송, 전시, 공연 및 방송할 수 있습니다.

다음과 같은 조건을 따라야 합니다:



저작자표시. 귀하는 원저작자를 표시하여야 합니다.



비영리. 귀하는 이 저작물을 영리 목적으로 이용할 수 없습니다.



변경금지. 귀하는 이 저작물을 개작, 변형 또는 가공할 수 없습니다.

- 귀하는, 이 저작물의 재이용이나 배포의 경우, 이 저작물에 적용된 이용허락조건을 명확하게 나타내어야 합니다.
- 저작권자로부터 별도의 허가를 받으면 이러한 조건들은 적용되지 않습니다.

저작권법에 따른 이용자의 권리는 위의 내용에 의하여 영향을 받지 않습니다.

이것은 [이용허락규약\(Legal Code\)](#)을 이해하기 쉽게 요약한 것입니다.

[Disclaimer](#)

Doctoral Thesis

Remote Detection of Radioactive Material on the
Basis of the Plasma Breakdown Using High-Power
Millimeter-Wave Source

Dongsung Kim

Department of Physics

Graduate School of UNIST

2017

Remote Detection of Radioactive Material on the Basis of the Plasma Breakdown Using High-Power Millimeter-Wave Source

Dongsung Kim

Department of Physics

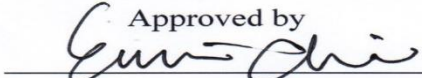
Graduate School of UNIST

Remote Detection of Radioactive Material on the Basis of the Plasma Breakdown Using High-Power Millimeter-Wave Source

A thesis
submitted to the Graduate School of UNIST
in partial fulfillment of the
requirements for the degree of
Doctor of Philosophy

Dongsung Kim

06. 21. 2017

Approved by


Advisor

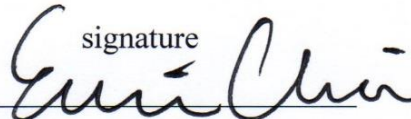
Eunmi Choi

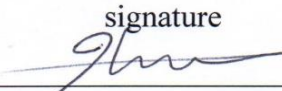
Remote Detection of Radioactive Material on the Basis of the Plasma Breakdown Using High-Power Millimeter-Wave Source

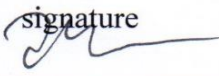
Dongsung Kim

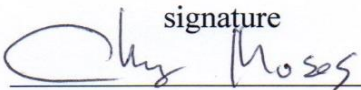
This certifies that the thesis/dissertation of Dongsung Kim is approved.

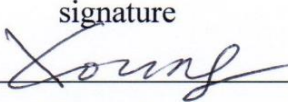
06. 21. 2017 of submission

signature

Advisor: EunMi Choi

signature

Min Sup Hur: Thesis Committee Member #1

signature

Kyujin Kwak: Thesis Committee Member #2

signature

Moses Chung: Thesis Committee Member #3

signature

Young-soon Bae: Thesis Committee Member #4;

Abstract

This thesis demonstrates the possibility of remote detection of radioactive material in long distance using high-power millimeter/THz wave source, gyrotron. It has been encouraged by a limitation of the current technologies which can only detect in short distance, about few meters, from the source. This proposed novel idea is based on ambient free electron density in the vicinity of the radioactive source. There are only a few free electrons in normal atmospheric air condition (~ 10 electrons/cm³). However, the electron density increases exponentially with radioactive material owing to the Compton scattering among the radiation from the source and air molecules. High density of average free electrons indirectly indicates the presence of the field enhancing factor such as radioactivity. The focused high-power millimeter-wave beam near the source induce the plasma avalanche ionization. As the millimeter-wave source, our laboratory-made gyrotron operates at 95 GHz and tens of kilowatts with 20 μ s of pulse duration. In the experiments, we concentrate on the plasma avalanche delay time, from an appearance of a seed electron up to the emission of the light induced by the breakdown discharge.

Beginning with the argon (Ar) discharge phenomena, plasma image, velocity, and spectroscopy were observed without external source. Based on the Paschen curve, which indicates the required electric field for the breakdown, the reduced threshold electric fields were experienced with a radioactive source. Besides, measurements of the eliminated statistical delay time lead to the existence of the radioactive material. Interestingly, even though the induced electromagnetic (EM) field was much lower than the threshold field, the attenuated radio frequency (RF) signal was measured in atmospheric air condition. These new experimental results were sufficient evidence to indicate the possibility of the remote detection of radioactive material.

By measuring the breakdown discharge induced by the high-power pulsed millimeter-wave radiation, the detection range of our method can be extended to the kilometer range involving with the proper size of an antenna and simply weak turbulence. Furthermore, the detection sensitivity of the method is 4000 times higher than that suggested by theoretical calculations; this is achieved by measuring the plasma breakdown delay time with plasma on/off phenomenon. Our results provide a technical breakthrough in the remote sensing of radioactive material, which should not only be useful in the development of high-power EM wave sources but also directly affect the security aspects of modern life.

Acknowledgement

우리 주 예수 그리스도의 하나님, 영광의 아버지께서 지혜와 계시의 영을 너희에게 주사 하나님을 알게 하시고 너희 마음의 눈을 밝히사 그의 부르심의 소망이 무엇이며 성도 안에서 그 기업의 영광의 풍성함이 무엇이며 그의 힘의 위력으로 역사하심을 따라 믿는 우리에게 베푸신 능력의 지극히 크심이 어떠한 것을 너희로 알게 하시기를 구하노라 (에베소서 1:17-19)

처음과 나중이며 시작과 끝인 하나님 아버지께서 많은 지혜와 사랑과 은혜를 베풀어 주셔서, 이렇게 졸업하도록 인도하여 주신 것에 감사드립니다.

2011년 1월, U-WURF를 시작으로 인연을 맺었던 연구실 생활을 2017년 8월 졸업을 앞두기까지 많은 가르침과 격려를 끊이지 않으셨던 최은미 지도교수님께 머리 숙여 깊이 감사드립니다. 학생들을 전적으로 신뢰하고, 크고 작은 어려움에 부딪힐 때마다 직접적인 해답을 제시하여 주시기보다는, 스스로 해결할 수 있는 능력과 해낼 수 있다는 자신감을 갖도록 지도하여 주신 교수님, 감사합니다. 그리고 항상 옆에서 같이 지내며 일했던 동료들인 TEE 연구실 사람들에게도 감사하다는 말을 전하고 싶습니다. 박사과정을 지나오면서, 열심히 연구하는 친구들의 모습이 저에게는 많은 자극이 되었으며 혼자서 할 수 없는 일들을 같이 이루어 나갈 때마다 친구들의 소중함을 느꼈습니다. 졸업 이후, 그 친구들에게 제가 조금이나마 힘이 될 수 있는 상황이 온다면, 기꺼이 기쁨 마음으로 도움이 되겠습니다.

어릴 적 매일 아침 눈을 뜨면, 공부하고 계시던 아버지의 모습을 보며 자라오면서 저의 학문의 길은 정해지지 않았나 싶습니다. 네 지혜를 의지하지 말고, 작은 일에도 주님께 구하고 감사하라고 가르치셨던 아버지·어머니, 현재의 주어진 상황에 감사하고 다른 사람에게 베푸는 삶을 사는 가르침을 주셨던 아버지·어머니, 영국에서 박사과정을 하며 항상 응원해주었던 형과 형수님, 힘들고 어려운 상황 속에서 끊임없는 격려와 학업을 마치고 육아에 전념하고 있는 아내, 장예은에게 감사하다는 말

을 전하고 싶습니다. 그리고 방사능 물질 원격 탐지에 관한 논문 리뷰 과정 중, 그만두고 주저앉고 싶을 때마다 포기하지 않고 끝까지 기도하며 응원해 주셨던 최창식 목장 식구들, 화평 초원 식구들, 그리고 목사님께 감사드립니다.

만 2살을 앞둔 아기 규현이가 자라서 이 글을 읽을 때쯤, 아들의 눈에 비추어질 아버지의 모습을 상상하며 최선을 다하며 살아가도록 하겠습니다. 하나님께서 주신 사명을 붙잡고 하루하루 주님께 의지하며 나아가 하나님께 영광 돌릴 수 있는 삶을 살도록 하겠습니다. 감사합니다.

2017.07.07.

김동성

Contents

I.	Introduction -----	15
1.1	Breakdown discharge -----	15
1.2	Gyrotron oscillator -----	16
1.3	Motivation -----	17
1.4	Thesis outline -----	18
II.	Theoretical & Mathematical Development -----	21
2.1	Estimation of plasma density for under-threshold condition -----	21
2.2	Theoretical derivation of delay time for Ar plasma -----	24
III.	Experimental Setup for Radioactive Material Detection -----	29
3.1	Components for plasma breakdown measurement -----	29
3.1.1	Focusing mirror -----	29
3.1.2	Chamber window -----	32
3.1.3	Detectors for incident RF wave and fluorescent light -----	35
3.1.4	Radioactive material; 0.64 mCi of ^{60}Co -----	36
3.2	Schematic design for plasma breakdown experiment -----	37
IV.	Results of Plasma Breakdown for Radioactive Material -----	41
4.1	Experimental results for Ar plasma breakdown -----	41
4.1.1	Plasma breakdown image -----	41
4.1.2	Plasma velocity -----	43
4.1.3	Spectroscopy -----	44
4.2	Experimental results for breakdown threshold electric field -----	45
4.3	Experimental results for delay time -----	47
4.3.1	Delay time in Ar condition -----	47
4.3.2	Delay time in air condition -----	52
4.4	Analysis of delay time measurement -----	55
4.4.1	Sensitivity of delay time -----	55
4.4.2	Reduction of required electric field with radioactive material -----	56
4.4.3	Possible detection ranges and limitation -----	60
V.	Conclusion -----	63
	References -----	65

List of Figures

1-1	A structure and typical elements of the gyrotron oscillator -----	16
1-2	Concept of remote radioactive material detection using a high-power (EM) wave, namely, a gyrotron, as an active source. A high-intensity EM beam is irradiated near the hazardous source, resulting in instantaneous plasma breakdown at the focal point due to the high average number of free electrons generated by the radioactive material- -----	18
2-1	Absorbing material placed between two dielectric materials -----	21
3-1	Normalized power of the microwave output beam at 95 GHz -----	30
3-2	Normalized power reflected from the focusing mirror. The location of the beam waist was $z=36.5$ cm -----	31
3-3	Beam pattern at focal point of $z=36.5$ cm. The beam size of w_x and w_y were 0.48 cm and 0.52 cm, respectively -----	31
3-4	Conceptual diagram for the chamber window -----	32
3-5	Design for the window of width d and its equivalent two ports -----	34
3-6	Calculated transmittance and reflection for 7.36 mm thickness of vacuum window ---	35
3-7	(a) The RF detector for incident wave and (b) photodiode detector for light emission of breakdown -----	36
3-8	The decay scheme of ^{60}Co . Two strong gamma photons are generated by decaying ---	37
3-9	(a) A disk type of ^{60}Co . (b) Auto-controlled lead chamber for radioactive material ----	37
3-10	Experimental setup for the measurement of plasma discharge delay time with radioactive material -----	38
4-1	Plasma image measurement for the measurement of plasma discharge delay time. (a) The fast camera is located on the right side of the chamber. (b) The EM wave propagates in z (k) direction. However, the plasma propagates in k' direction opposite direction of the incident wave because the plasma performed like a conductor and intensity of the beam was high along the opposite direction after plasma occurs at focal point -----	42
4-2	Plasma velocity measurement using the ICCD camera. (a) Experimental setup for the plasma velocity. (b) Movement of the plasma formation in different time interval ----	43
4-3	Spectroscopy measurement in Ar plasma using spectrometer. (a) Measurement setup for the Ar plasma. (b) Spectroscopy result shows that the spectrum signal induced by	

	the fluorescent light is near 700 nm -----	44
4-4	Theoretical Paschen curve and experimental measurement of threshold electric field for breakdown in Ar and air -----	46
4-5	Amplitude of the RF signal under different pressure in Ar and air -----	47
4-6	Survival rate for an incident RF wave during pulse duration. The experimental data are shown without radioactive material (blue circles) and with radioactive material (red crosses). The black dotted line indicates the fit curve for the presence of radioactive material case using equation (2.28) -----	48
4-7	Real time measurement of delay time with and without radioactive material. The gyrotron operates at 19 kW and 250 Torr. The lead gate was opened and closed every 30 seconds to appear the radiation of ⁶⁰ Co. The minimum delay time in each circumstance were 2.2 μs and 4.1 μs -----	49
4-8	Real time measurement of delay time with and without radioactive material. As the distance increases from 20 cm to 120 cm, the dispersion of the delay time also spreads further -----	50
4-9	The probability of plasma breakdown and average number of free electrons using MCNPX code. This experiment is performed at 28 kW in 400 Torr of Ar gas. The experimental result of probability decreases exponentially with increasing distance. The reason of reduction is owing to the decrease of the average number of free electrons -----	51
4-10	The experimental results in under-threshold condition. (a) Total probability for breakdown discharge as a function of time. (b) Delay time distribution with and without source at 30 and 32 kW. (c) Delay time distribution in different output power at 30 and 760 Torr -----	52
4-11	The experimental results in under-threshold condition in air. (a) & (b) Total probability for breakdown discharge as a function of delay time. (c) & (d) Delay time distribution with radioactive source at 30 and 32 kW. The hatched areas show the ambient condition so that plasma breakdown does not occur. (e) Delay time distribution in various output power at 60 and 760 Torr -----	54
4-12	Production rate of electrons for 0.64 mCi of ⁶⁰ Co located 20 cm away from center of the RF beam. The energy spectrum was calculated using MCNPX ver 2.50 code -----	59
4-13	Electric field reduction factor (β) as a function of average free electron density -----	59
4-14	Possible detection ranges of radioactive material using high-power microwave source. The radioactive source is shielded in container -----	60

List of Tables

3-1	Design parameters of the vacuum chamber -----	33
4-1	Calculated plasma densities using the attenuated RF signal in different condition-	47
4-2	Comparable detection ranges in current technology and proposed method using delay time -----	61

Abbreviations and Acronyms

Ar	Argon
Co	Cobalt
EM	Electromagnetic wave
ICCD	Intensified charge-coupled device
MCNPX	Monte Carlo N-Particle eXtended
RDD	Radiological dispersal device
RF	Radio frequency
THz	terehertz

Chapter 1

Introduction

1.1 Breakdown discharge

Electrical discharge in gas has been studied in several areas of science. An electric field of two electrodes containing a gas produces the electrons and ions separately. If the applied field is sufficient to convey the energy, the electrons produce secondary electrons due to the collision. That is to say, the secondary electrons are created, and the gas becomes acting like a conductor. In a gas discharge, the ionization, diffusion, and recombination are performed. When the production rate of electrons is little higher than loss rate, the electron concentration increases exponentially and achieves the breakdown discharge with light emission. The spurious electrons or external electrons for sustaining this process start to form the breakdown.

In 1900s, the gas discharges field was established as a school in the physics by John Sealy E. Townsend (1868-1957), and discovered the fundamental theory of ionization and gas discharge known as Townsend discharge. The motion of electrons in gases, including electron-ion collisions, drift velocities of electrons and ions, and other research were shown as experimental results. Irving Langmuir (1881-1957) introduced the concept of a plasma in 1928. He studied the light emission from the charged particles and developed how to measure the electron temperature and electron density with an electrostatic probe called Langmuir probe. In 1940 ~ 1950, Sanborn C. Brown and Melvin A. Herlin introduced the gas discharge in the microwave regime, and beginning of the breakdown experiments was accomplished with noble gases instead of air owing to the complex chemical structure and physical reaction in air molecules. In the microwave regime, theoretical and experimental approaches to gaseous plasma breakdown in the atmosphere improved by A.D. Macdonald in the 1960s [1]. Based on the properties of atmospheric particles and theoretical analysis of the complicated chemical structure of microwave frequencies, the experimental conditions were established for widespread measurement of gas breakdown. Recently, this kind of the plasma breakdown has been conducted using the sub-THz

gyrotron to generate at high-power and high frequencies [2]–[8].

1.2 Gyrotron oscillator

As the gyrotron is one of the vacuum electron devices, electromagnetic (EM) waves of high-power and high frequencies are generated by converting the energy of the electron beam to EM wave energy. This device consists of an electron gun, a resonant cavity, a mode converter, output window, and collector as shown in Fig. 1-1. The energetic electron beam is generated at the electron gun and pass through the beam tunnel. A magnetic field is utilized to guide and control the electron beam before the entrance of the resonant cavity. The guided beam interacts at the inhomogeneous media which is associated with the resonant structure in cavity to generate the millimeter/THz wave. In other words, the electron’s axial energy provides condition for synchronism and bunching, and with the electron cyclotron resonance, the electron beam conveys their kinetic energy to the coherent EM wave through azimuthal interaction [9]. The electrons that lose energy are discarded at the collector, and the generated wave with cylindrical cavity mode is converted to linearly polarized Gaussian-like beam at the quasi-optical mode converter. The radiated beam is guided by mirrors and propagates through the transparent window. The output beam of the gyrotron arrives at the waveguides or used for numerous areas in nuclear fusion reaction, material and biological science, medical industry, and military applications.

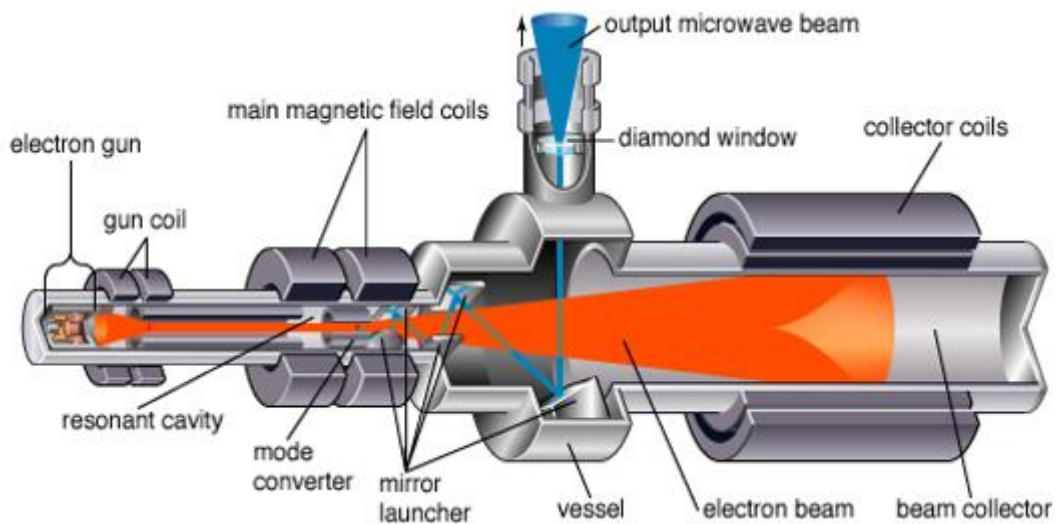


Figure 1-1: A structure and typical elements of the gyrotron oscillator [10]

1.3 Motivation

Radioactive material is widely used in our daily life from diagnosis and therapy of cancer in nuclear power plants and nuclear weapons. In some cases, the abuse of radioactivity is worried among people. For example, there was also a guy who sent a drone containing radioactive material to Japan's prime minister's office, and the threats using radioactive material are used for radiological dispersal devices (RDD), called dirty bombs. Moreover, a radiation leak from the nuclear power station in Japan was a tremendous accident, so that the areas have been restricted from human beings owing to the radiation exposure. New advanced skills are required to solve this problem since a limitation of current technology is that the maximum distance to measure the 1 milliCurie (mCi) of Cobalt-60 (^{60}Co) radioactive material is about 3.5 m away from the source; we define the hazardous level to human health is $1 \mu\text{Sv/h}$. Not only the investigator should be exposed from the radiation but also the detection range is too short to approach the contaminated areas.

A novel idea is initiated by the University of Maryland using high-power terahertz (THz)-wave source to detect the radioactive source in long distance. Figure 1-2 illustrates the underlying detection mechanism [11]–[13]. This method is related to the number of free electrons in the vicinity of the dangerous material. Small quantity of free electrons ($1\text{--}10 \text{ electrons/cm}^3$) are exist in ambient air condition, and theoretically the probability to have one seed electron in the breakdown-prone volume of 0.16 cm^3 at 670 GHz is about 14 %. If there is an external source such as UV-lamp or field enhancing material, the probability exceeds more than that owing to the presence of created free electrons inside of the breakdown-prone volume. Of course, the EM wave above the threshold electric field to initiate the plasma avalanche effect is essential.

Our new approach is dependent on plasma avalanche delay time [12], [14]–[16]. The compulsory time to reach the plasma formation state is required to initiate the avalanche breakdown. However, the radioactive material generated free electrons by the Compton scattering of strong gamma-rays and enhance the density of free electrons in the vicinity of the focused millimeter-wave area. The essential time can be decreased comparing the ambient condition (normal state). Neither the high frequency nor the small breakdown-prone volume are not mandatory to perform our detection method using delay time. The remote detection of radioactive material using real source has not yet been clarified using high-power source. Thus, the priority of this thesis is to demonstrate the feasibility of detecting radioactive materials in long distance.

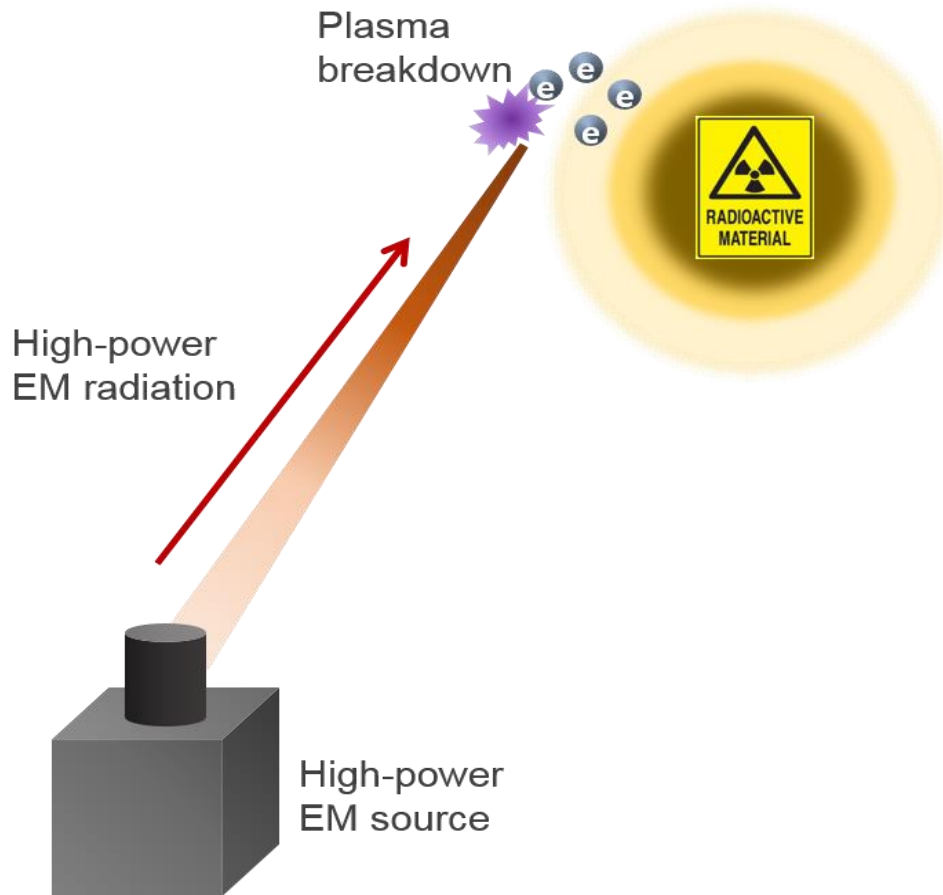


Figure 1-2: Concept of remote radioactive material detection using a high-power EM wave, namely, a gyrotron, as an active source. A high-intensity EM beam is irradiated near the hazardous source, resulting in instantaneous plasma breakdown at the focal point due to the high average number of free electrons generated by the radioactive material [12].

1.4 Thesis outline

After introducing the reason of this plasma breakdown experiment, a theoretical calculation of underdense plasma density and total delay time composed of formative and stochastic delay time are described in Chapter 2. Chapter 3 consists of the components for measurement of plasma breakdown delay time, including focusing mirror, vacuum chamber, RF detector, photodiode detector, and radioactive material as ^{60}Co . We also show the experimental schematic for the plasma breakdown. All the results about plasma discharge are described in Chapter 4. First, the argon (Ar) plasma image, plasma velocity in Ar gas, and spectroscopy of Ar plasma. Next, the threshold electric field based on

Paschen's law and delay time results are presented. At the end of this chapter, we point out the analysis of delay time measurement. The conclusion of this dissertation is stated in Chapter 5.

Chapter 2

Theoretical & Mathematical Development

2.1 Estimation of plasma density for under-threshold condition

There are two kinds of plasma structure; the plasma performs as a mirror in the overdense case which the angular frequency (ω) is smaller than the plasma frequency (ω_p). The other is the underdense structure when the angular frequency is larger than the plasma density so the plasma acts like a nonlinear refractive medium. Here, we introduce the underdense plasma state to consider the attenuated RF wave between two dielectric media [17]. Let's assume that the incident RF wave penetrates a conductor as shown in Fig. 2-1. The incident EM wave is stratified dielectric media and not completely absorbed by the conductor.

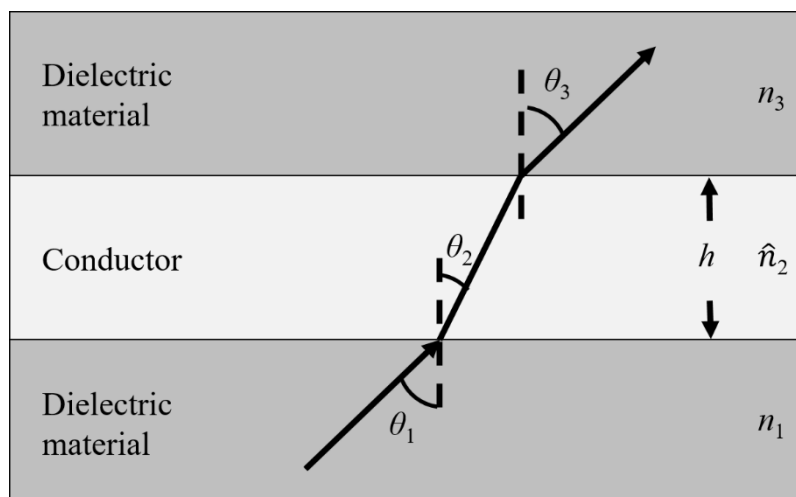


Figure 2-1: Absorbing material placed between two dielectric materials [17].

The complex refractive index of conductor is given by

$$\hat{n}_2 = n_2(1 + i\kappa_2), \quad (2.1)$$

where \hat{n}_2 and κ_2 are the real and the imaginary part, respectively. Hence, we obtain an expression for the dielectric constant of a plasma is written as

$$\varepsilon = 1 - \frac{\omega_p^2}{\omega^2 + i\omega\nu_{\text{eff}}}, \quad (2.2)$$

where ν_{eff} is the effective collision frequency of the electrons [18]. Thus, the incident wave takes the form of decaying wave. The electron density is increased from 1 cm^{-3} about to be exponential growth with time. Thus, the real and imaginary parts of the refractive index can be written as

$$n_2 = \sqrt{\frac{(\varepsilon)_{\text{re}}}{2} + \sqrt{\left(\frac{(\varepsilon)_{\text{re}}}{2}\right)^2 + \left(\frac{(\varepsilon)_{\text{im}}}{2}\right)^2}} \quad (2.3)$$

and

$$\kappa_2 = \sqrt{-\frac{(\varepsilon)_{\text{re}}}{2} + \sqrt{\left(\frac{(\varepsilon)_{\text{re}}}{2}\right)^2 + \left(\frac{(\varepsilon)_{\text{im}}}{2}\right)^2}}. \quad (2.4)$$

To calculate the refractive index of the conductor media, the following expression is given by

$$\hat{n}_2 \cos \theta_2 = u_2 + iv_2, \quad (2.5)$$

$$\text{and } \hat{n}_2 \sin \theta_2 = n_1 \sin \theta_1, \quad (2.6)$$

where u_2 and v_2 are real values. Substituting the equation of Snell's law (2.6) into squaring equation of (2.5), it's simply written as

$$(u_2 + iv_2)^2 = (\hat{n}_2)^2 - (n_1 \sin \theta_1)^2. \quad (2.7)$$

Each component of real and imaginary part from the above equation (2.7) is followed as

$$u_2^2 - v_2^2 = n_2^2 (1 - \kappa_2^2) - n_1^2 \sin^2 \theta_1 \quad (2.8)$$

$$u_2 v_2 = n_2^2 \kappa_2$$

For the TE wave, the reflection and transmission coefficient at the first interface are given by

$$r_{12} = \rho_{12} e^{i\phi_{12}} = \frac{n_1 \cos \theta_1 - (u_2 + i v_2)}{n_1 \cos \theta_1 + (u_2 + i v_2)} \quad (2.9)$$

$$\rho_{12}^2 = \frac{(n_1 \cos \theta_1 - u_2)^2 + v_2^2}{(n_1 \cos \theta_1 + u_2)^2 + v_2^2} \quad (2.10)$$

$$\tan \phi_{12} = \frac{2v_2 n_1 \cos \theta_1}{u_2^2 + v_2^2 - n_1^2 \cos^2 \theta_1}$$

$$t_{12} = \tau_{12} e^{i\chi_{12}} = \frac{2n_1 \cos \theta_1}{n_1 \cos \theta_1 + (u_2 + i v_2)} \quad (2.11)$$

$$\tau_{12}^2 = \frac{(2n_1 \cos \theta_1)^2}{(n_1 \cos \theta_1 + u_2)^2 + v_2^2} \quad (2.12)$$

$$\text{and } \tan \chi_{12} = -\frac{v_2}{n_1 \cos \theta_1 + u_2}$$

where ρ_{12} and τ_{12} are amplitudes, and ϕ_{12} and χ_{12} are phase changes. Likewise, the amplitudes ρ_{23} and τ_{23} are amplitudes, and ϕ_{23} and χ_{23} are phase changes at the second boundary for the reflection and transmission coefficients which are given by

$$\rho_{23}^2 = \frac{(n_3 \cos \theta_3 - u_2)^2 + v_2^2}{(n_3 \cos \theta_3 + u_2)^2 + v_2^2} \quad (2.13)$$

$$\tan \phi_{23} = \frac{2v_2 n_3 \cos \theta_3}{u_2^2 + v_2^2 - n_3^2 \cos^2 \theta_3}$$

$$\tau_{23}^2 = \frac{4(u_2^2 + v_2^2)}{(n_3 \cos \theta_3 + u_2)^2 + v_2^2}, \quad (2.14)$$

$$\text{and } \tan \chi_{23} = \frac{v_2 n_3 \cos \theta_3}{u_2^2 + v_2^2 + u_2 n_3 \cos \theta_3}.$$

Combining the equations from (2.9) to (2.14), the solution for the reflectance and transmittance is written as

$$R = |r|^2 = \frac{\rho_{12}^2 e^{2v_2 \eta} + \rho_{23}^2 e^{-2v_2 \eta} + 2\rho_{12}\rho_{23} \cos[\phi_{23} - \phi_{12} + 2u_2 \eta]}{e^{2v_2 \eta} + \rho_{12}^2 \rho_{23}^2 e^{-2v_2 \eta} + 2\rho_{12}\rho_{23} \cos[\phi_{12} + \phi_{23} + 2u_2 \eta]} \quad (2.15)$$

and

$$T = \frac{n_3 \cos \theta_3}{n_1 \cos \theta_1} |t|^2 = \frac{n_3 \cos \theta_3}{n_1 \cos \theta_1} \cdot \frac{\tau_{12}^2 \tau_{23}^2 e^{-2v_2 \eta}}{1 + \rho_{12}^2 \rho_{23}^2 e^{-4v_2 \eta} + 2\rho_{12}\rho_{23} e^{-2v_2 \eta} \cos[\phi_{12} + \phi_{23} + 2u_2 \eta]}, \quad (2.16)$$

where $\eta = 2\pi h/\lambda_0$, h and λ_0 are the thickness of the conductor and the wavelength in a vacuum, respectively. Based on the formalism described in this section, the plasma density will be calculated using the measurement transmittance values during the experiment in section 4.2.1.

2.2 Theoretical derivation of delay time for Ar plasma

It takes a certain time for the plasma discharge to occur. We name it as the total delay time, which consists of the formative delay time and statistical delay time. This is an essential parameter to determine the existence of radioactive material. The formative delay time represents a time for exponential growth of a primary seed electron to that of avalanche ionization. First, we derive the formative delay time from the continuity equation of the electron. The electron density at a time (t) is written as

$$n(t) = n_i \exp[\nu t]. \quad (2.17)$$

where n_i is the initial density of free electrons; $\nu = \nu_i - \nu_a - \nu_d$ is the net ionization frequency. The ν_i , ν_a , and ν_d represent the ionization, attachment, and diffusion frequencies, respectively. The ionization frequency for inelastic collisions, ν_i , is given by [19]

$$\nu_i = a^2 \times \nu_E \times \alpha \times \beta, \quad (2.18)$$

$$\alpha = 2 \times a \times \exp\left(-\frac{a-1}{a} \times \sqrt{\frac{6\nu^*}{\nu_E}}\right), \quad (2.19)$$

and

$$\nu_E = 1.75 \times 10^{15} \times \left(\frac{E_{rms}^2}{\omega^2 + \nu_m^2}\right) \times \frac{\nu_m}{I_1}, \quad (2.20)$$

Here, $a = 1.2$ is for monatomic gases; $\beta = 0.2$ is for heavy frequencies like millimeter or long wave of infrared radiation; $\nu^* = 2.6 \times 10^8 \times p$ (Torr/s) is the atomic excitation frequency for Ar gas, $\nu_m = 7 \times 10^9 \times p$ (Torr/s) is the elastic collision frequency of electrons and Ar, p is the inner pressure of the chamber; E_{rms} is the root-mean-square electric field of incident EM wave; and $\omega = 2\pi f$ (rad/s) is the angular frequency of the RF beam.

The drift diffusion frequency is as follows:

$$\nu_d = \frac{D}{\Lambda^2} = \frac{5.8 \times 10^{14} \times I^*}{\nu_m \times \Lambda^2}, \quad (2.21)$$

where D is the diffusion coefficient of free electron, $\Lambda = \omega_0/\pi$ is the specific diffusion length defined by the beam waist (ω_0), and $I^* = 11.5$ eV is the energy of metastable Ar molecules. The probability of an avalanche reaching a size of N electrons is given by [19,20]

$$P(N) = \frac{1}{n} \exp\left(-\frac{N}{n}\right), \quad (2.22)$$

where \bar{n} (cm^{-3}) is the average electrons of N when $n_i = 1$ electron/ cm^3 in equation (2.17) which is written as

$$\bar{n} = \exp\left[\int_0^t (\nu_i(t') - \nu_d) dt'\right], \quad (2.23)$$

Substituting equations (2.23) into equation (2.22), the probability to notice N electrons in an avalanche ionization is

$$P(N) = \left(\frac{1}{\exp\left[\int_0^t (\nu_i(t') - \nu_d) dt'\right]} \right) \exp\left(-\frac{N}{\exp\left[\int_0^t (\nu_i(t') - \nu_d) dt'\right]} \right). \quad (2.24)$$

To find the probability within specific delay time is determined when the plasma frequency is the same as the angular frequency of our gyrotron ($f \approx 95$ GHz) which indicates that the electron density achieve the critical electron density ($n_{cr} \approx 10^{14}/\text{cm}^3$).

$$P_1(N < n_{cr}, t) = \int_0^{n_{cr}} P(N) dN = 1 - \exp\left(-\frac{n_{cr}}{n}\right). \quad (2.25)$$

The derived probability based on the formative delay time is a function of the amplitude of the electric field and the pressure.

Second, the seed electron is not always present in the breakdown-prone volume, and the plasma avalanche ionization takes place with a random delay time which means that there is a required time to presence of the seed electron called statistical delay time. However, the presence of the radioactive material indicates that the statistical delay time always has the same distribution formula due to the free electrons generated by the radioactive material. In other words, the statistical delay time has small distribution in the presence of radioactivity due to the increase in the average free electron density, and the probability of statistical delay time using the Poisson distribution is given by [5,15]

$$P_2(n) = \frac{1}{n!} (S\Delta t)^n \exp(-S\Delta t), \quad (2.26)$$

where S is the average generation rate of free electrons by the seeding source in the volume. Due to the presence of the radioactive material, the S term should be permanently stable to fit

the experimental distribution. The probability to discover the initial seed electron during time t is

$$P_2(n=0, t) = \exp(-St). \quad (2.27)$$

The time described from the appearance of the seed electron to reach the avalanche ionization state is defined as the delay time with pulse length t , written as

$$P = P_1 + P_2. \quad (2.28)$$

Therefore, the equation (2.28) represents the total delay time which is summation of the formative delay time and statistical delay time. This theoretical calculation will be used for comparing the plasma breakdown experimental results.

Chapter 3

Experimental Setup for Radioactive Material Detection

3.1 Components for plasma breakdown measurement

3.1.1 Focusing mirror

A small focused beam is required to initiate the plasma breakdown based on the threshold electric field density. The propagated beam path and shape from the gyrotron are illustrated in Fig. 3-1. An electric field integral equation code ‘Surf3d’ is used for the design of a focusing mirror [22]. In theoretically, the smallest beam waist is almost same as the wavelength of incident RF wave. The spherical mirror equation is given by

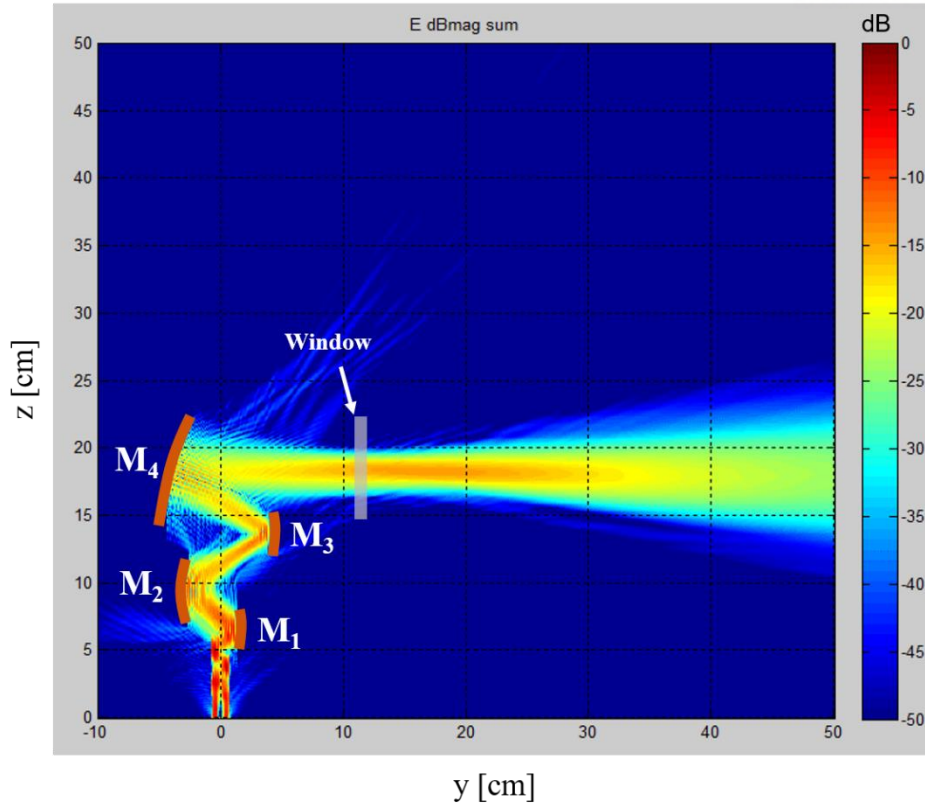


Figure 3-1: Normalized power of the microwave output beam at 95 GHz

$$z = \sqrt{R_x^2 - x^2} + \sqrt{R_y^2 - y^2} - (R_x + R_y) \quad (3.1)$$

where R_x and R_y are the radius of mirror curvature in each direction. Based on the property of the output beam from the gyrotron window and calculation using quasi-optical equation, the curvature of R_x and R_y are determined by 19 cm and 37 cm, respectively. The location of the focusing mirror is at 60 cm from the gyrotron center shown in Fig.3-2. The incident beam from the window is reflected and focused 18.5 cm away from the center of the focusing mirror. At this point, the propagated beam waist of w_x and w_y are 0.48 cm and 0.52 cm up to -8.7 dB similar as 1.6 times of wavelength illustrated in Fig. 3-3. This simulation result is small discrepancy of theoretical calculation since the EM wave from the gyrotron window is not perfectly Gaussian beam.

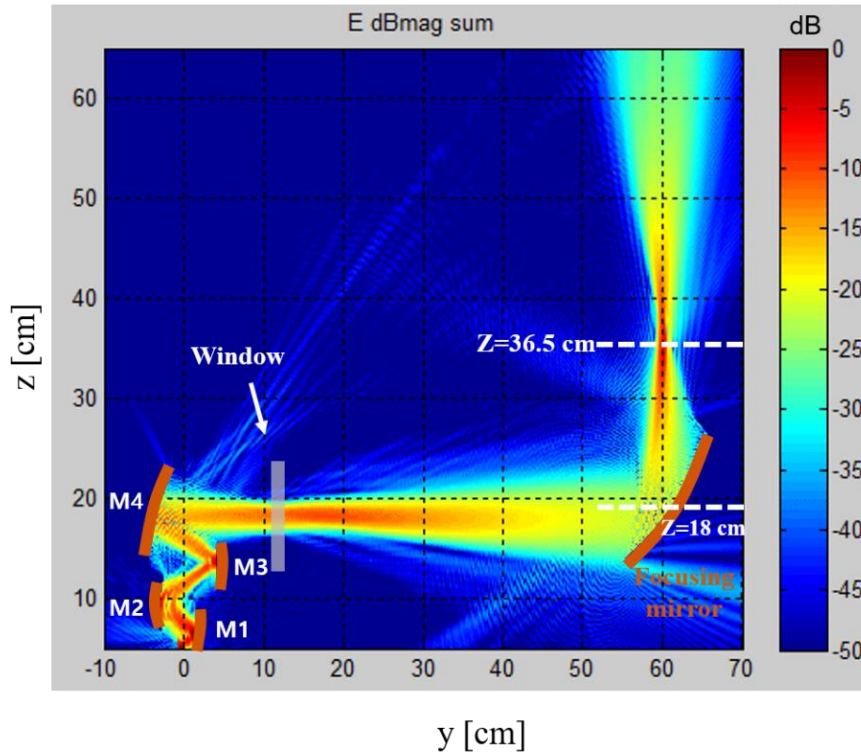


Figure 3-2: Normalized power reflected from the focusing mirror. The location of the beam waist was $z=36.5$ cm.

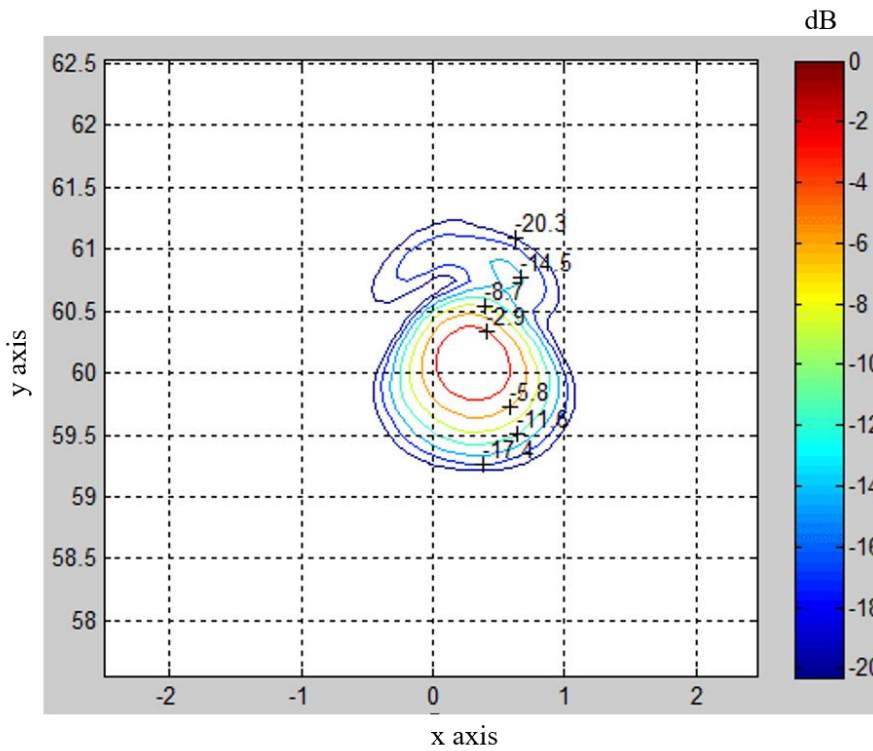


Figure 3-3: Beam pattern at focal point of $z=36.5$ cm. The beam size of w_x and w_y were 0.48 cm and 0.52 cm, respectively.

3.1.2 Chamber window

The plasma breakdown condition considered here required pressurized vacuum chamber filled with Ar gas because the output power of our laboratory-made gyrotron was tens of kilowatt regime which indicates the lack of threshold power to initiate the volume breakdown in the air. When we determine a window material for the vacuum chamber, the most important parameters are the transmittance and the absorption. A fused silica (SiO_2) was chosen as the window material which was same as the gyrotron's window. To calculate the thickness and aperture size, we first derive the equation for a minimum thickness of the window which is required to withstand an outer pressure [23]. (see Fig. 3-4)

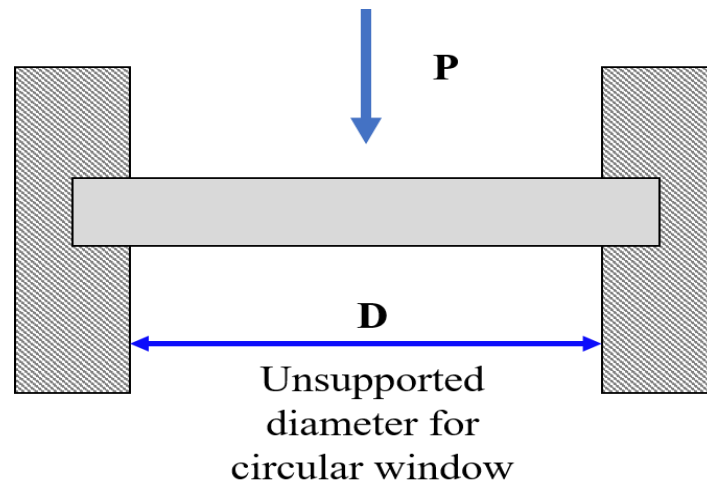


Figure 3-4: Conceptual diagram for the chamber window.

The maximum strength of the window is derived by

$$S_{\max} = \frac{K \times D^2 \times P}{4 \times T^2} = \frac{F_a}{SF} \quad (3.2)$$

where K is the empirical constant for clamped window, D is the unsupported diameter for circular window, P is the external pressure, T is the thickness of the window, F_a is the rupture modulus, and SF is the safety factor of the window material. The fused silica is used for the material of the window same material of the gyrotron's window. The final equation for the thickness of the window is given by

$$T = D \times \sqrt{\frac{K \times P \times SF}{4 \times F_a}}. \quad (3.3)$$

The main parameter values for this calculation are summarized in Table 3.1.

Table 3-1: Design parameters of the vacuum chamber

<i>SF</i> (Safety factor)	8
<i>F_a</i> (Apparent elastic limit)	7980 psi
<i>D</i> (Unsupported diameter for circular window)	14 cm
<i>K</i> (Empirical constant for clamped window)	0.75
<i>P</i> (Pressure)	14.7 psi
<i>T</i> (Thickness of window)	7.36 cm

Second, we also calculate the transmittance and reflectance for the proper size of the window [24]. Figure 3-5 shows a schematic design and scattering matrix. For a single RF window, the scattering matrix [S] is written as

$$[S] = \begin{bmatrix} S_{11} & S_{12} \\ S_{21} & S_{22} \end{bmatrix} = \begin{bmatrix} \frac{b_1}{a_1} & \frac{b_1}{a_2} \\ \frac{b_2}{a_1} & \frac{b_2}{a_2} \end{bmatrix}. \quad (3.4)$$

The transmittance (*T*) and reflectance (*R*) are given by the equation (3.4)

$$T = |S_{11}|^2 = \frac{P_{tran}}{P_{in}} = \frac{|b_2|^2}{|a_1|^2}$$

$$R = |S_{21}|^2 = \frac{P_{ref}}{P_{in}} = \frac{|b_1|^2}{|a_1|^2}. \quad (3.5)$$

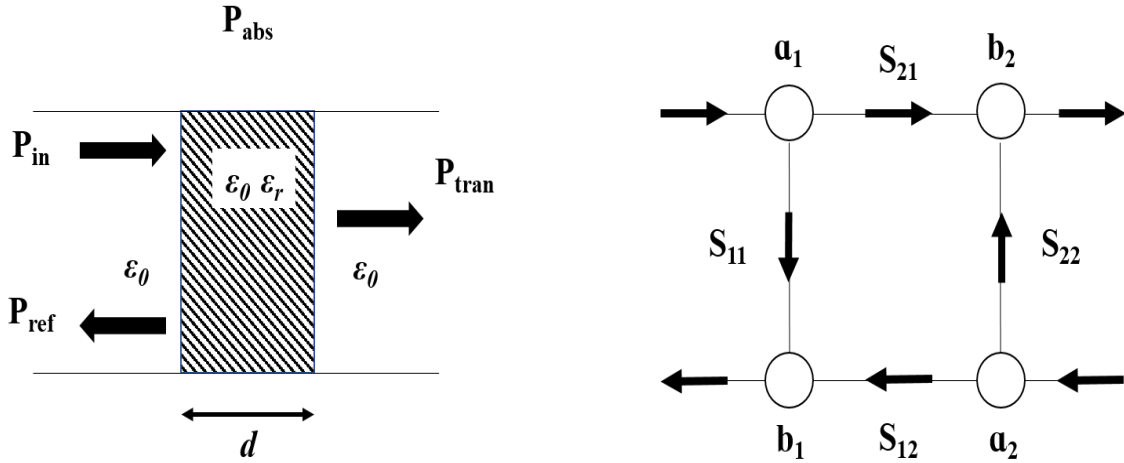


Figure 3-5: Design for the window of width d and its equivalent two ports. [24]

Thus, the scattering matrix $[S]$ is given by

$$[S] = \frac{1}{(1 - \rho_{mn}^2 \cdot e^{-2\gamma_{mn}d})} \begin{bmatrix} \gamma_{mn}(1 - e^{-2\gamma_{mn}d}) & (1 - \gamma_{mn}^2)e^{-\gamma_{mn}d} \\ (1 - \gamma_{mn}^2)e^{-\gamma_{mn}d} & \gamma_{mn}(1 - e^{-2\gamma_{mn}d}) \end{bmatrix} \quad (3.6)$$

where the propagation constant is written as $\gamma_{mn} = \alpha_{mn} + i\beta_{mn} = \sqrt{k_{cnn}^2 - \epsilon_r k_0^2}$, $k_{cnn} = \frac{x_{mn}}{D}$, and $k_0 = \frac{2\pi f}{c_0}$.

α_{mn} and β_{mn} are the attenuation and phase constants, respectively. Here, x_{mn} is the Bessel zero of the mode, and D is the diameter of the window. For TEM mode, the complex reflection coefficient is given in short form,

$$\rho_{mn} = \frac{1 - \sqrt{\epsilon_r}}{1 + \sqrt{\epsilon_r}} \quad (3.7)$$

Combining the above equations from (3.4) to (3.7), the T and R are given as

$$T = \frac{T_0(1 - 2R_0 \cos(2\phi) + R_0^2)}{1 - 2R_0 T_0 \cos(2\beta_{cnn}d - 2\phi) + R_0^2 T_0^2} \quad (3.8)$$

$$R = \frac{R_0(1 - 2T_0 \cos(2\beta_{cnn}d) + T_0^2)}{1 - 2R_0 T_0 \cos(2\beta_{cnn}d - 2\phi) + R_0^2 T_0^2}$$

where $T_0 = e^{-2\alpha_{mn}d}$, $R_0 = |\rho_{mn}|^2$, and $\phi = \arg \rho_{mn}$. With analysis of dielectric constant 3.8 and tangent loss 2×10^{-4} of fused silica, the thickness and aperture of the window are determined as 7.36 mm and 140 mm for the 0.95 of transmittance at 95 GHz (see Fig. 3-6). The chamber windows are located in both front and back side of chamber.

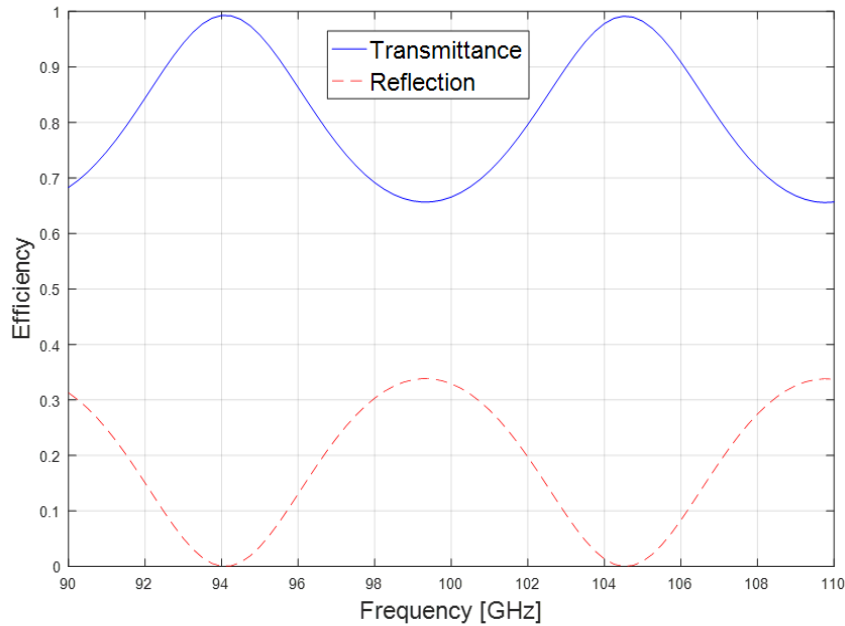


Figure 3-6: Calculated transmittance and reflection for 7.36 mm thickness of vacuum window.

3.1.3 Detectors for incident RF wave and fluorescent light

As previously introduced in Section 2.2, the total delay time is a priority factor in our experiments. This measurement is performed using W-band standard waveguide with twister for the direction of the electric field. We also prepare the one fixed 20 dB attenuator and one variable attenuator with detector by Millitech Incorporated, model DET-10 to modulate the incoming signal from the output power of the gyrotron. A Si avalanche photodiode (APD) is for the optical signal of plasma breakdown by Hamamatsu Photonics, model c12702-11(S12053 module). The APD has less than 2 ns rise time, and the spectral response range is from 200 nm to 1000 nm which is adequate to observe the Ar gas plasma occurred beyond a wavelength of 700 nm.

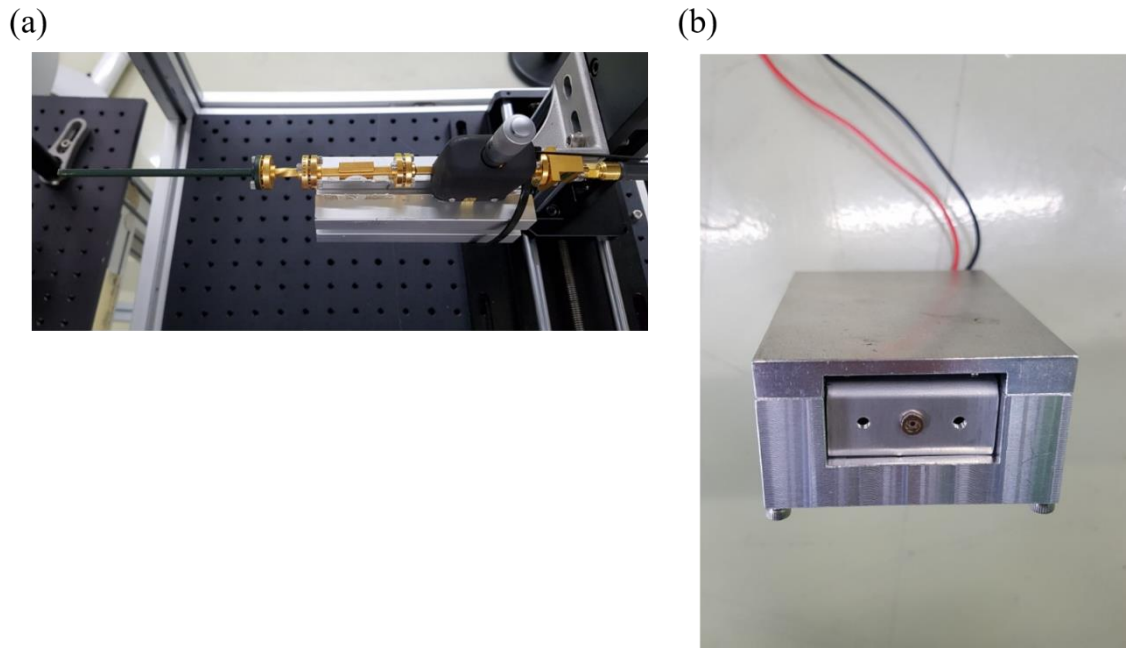


Figure 3-7: (a) The RF detector for incident wave and (b) photodiode detector for light emission of breakdown

3.1.4 Radioactive material; 0.64 mCi of ^{60}Co

A radioactive source is selected as Cobalt-60 (^{60}Co) which is typically used in hospital and is representative material of RDD. ^{60}Co has a relatively long half-life, 5.27 year, among the other radioactive material which emitted high intensity of gamma-rays. Originally, the ^{60}Co does not exist in a natural state, and a slow neutron is added to be a meta-stable or excited state. [ref Wikipedia]. When the radioactivity decays to daughter atom, the particles, electrons and photons, are produced and radiated in all direction. On the decay scheme of ^{60}Co , the generated gamma photons have strong energy of 1.173 MeV and 1.332 MeV with a probability of 99.9% as shown in Fig. 3-8. The energetic gamma-rays created by the radioactive source produce hundreds or thousands of free electrons in the ambient condition owing to the Compton scattering. In our experiment, a disc type of radioactive material is adopted and is positioned in center of the lead chamber hole (see Fig. 3-9).

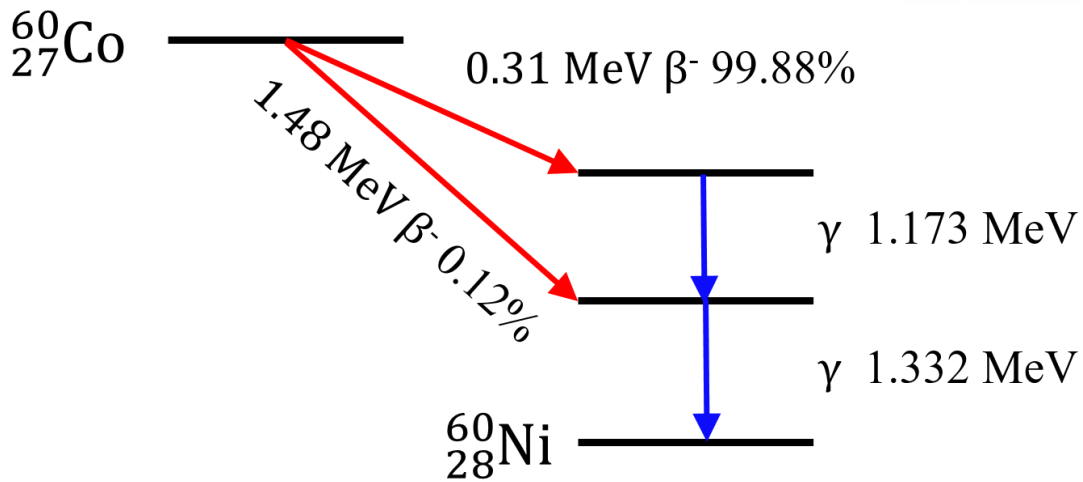


Figure 3-8: The decay scheme of ^{60}Co . Two strong gamma photons are generated by decaying

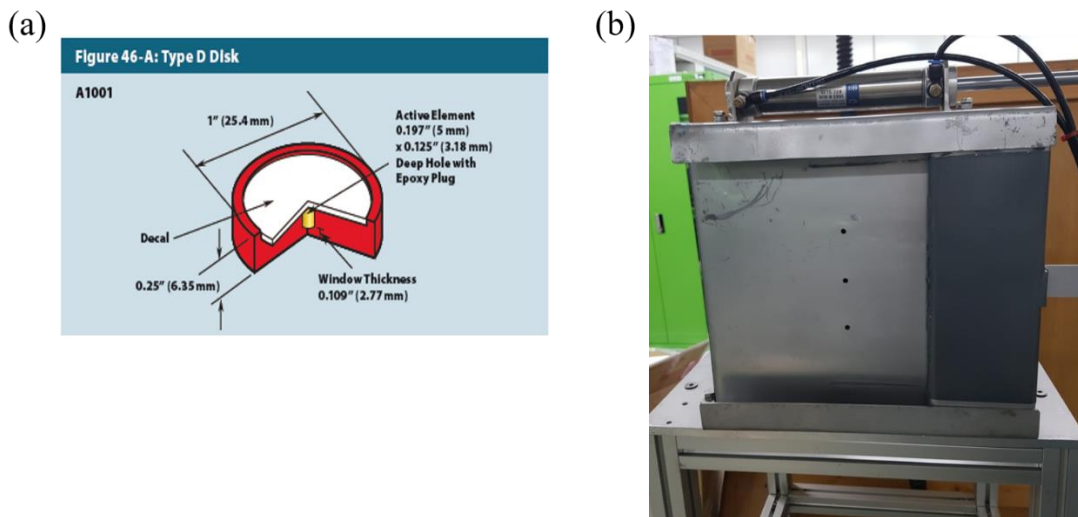


Figure 3-9: (a) A disk type of ^{60}Co . (b) Auto-controlled lead chamber for radioactive material.

3.2 Schematic design for plasma breakdown experiment

Figure 3-10 illustrates the schematic design for the measurement of the plasma volume discharge experiment. The gyrotron operates about 30 kW output power, 20 μs pulse duration with a frequency of 95 GHz [25]. An output Gaussian beam propagates from the gyrotron window and focuses at the center of pressurized vacuum chamber which is filled with Ar gas. By analyzing the simulation results and

measurement of beam size from the gyrotron window, the focused beam waist is about 1.6 times of the wavelength, which is same as 5mm. As mentioned in section 3.1.2, the incident electric field is not sufficient to initiate the plasma breakdown in atmospheric air condition, so the breakdown regime is varied from 3 Torr to 250 Torr with Ar gas. Inner pressure filled with Ar gas is maintained during the measurement time by supplying the Ar gas and extracting it at the same time. A distance from the radioactive source to the breakdown center is varied from 20 cm to 120 cm. With analysis of relationship between the presence of the radioactive material and the required electric field, the various pressurized condition is required to study for statistics. Our preliminary experiment is performed in normal condition, which indicates the case without radioactive material, to provide the reference data comparing the case of the radioactivity.

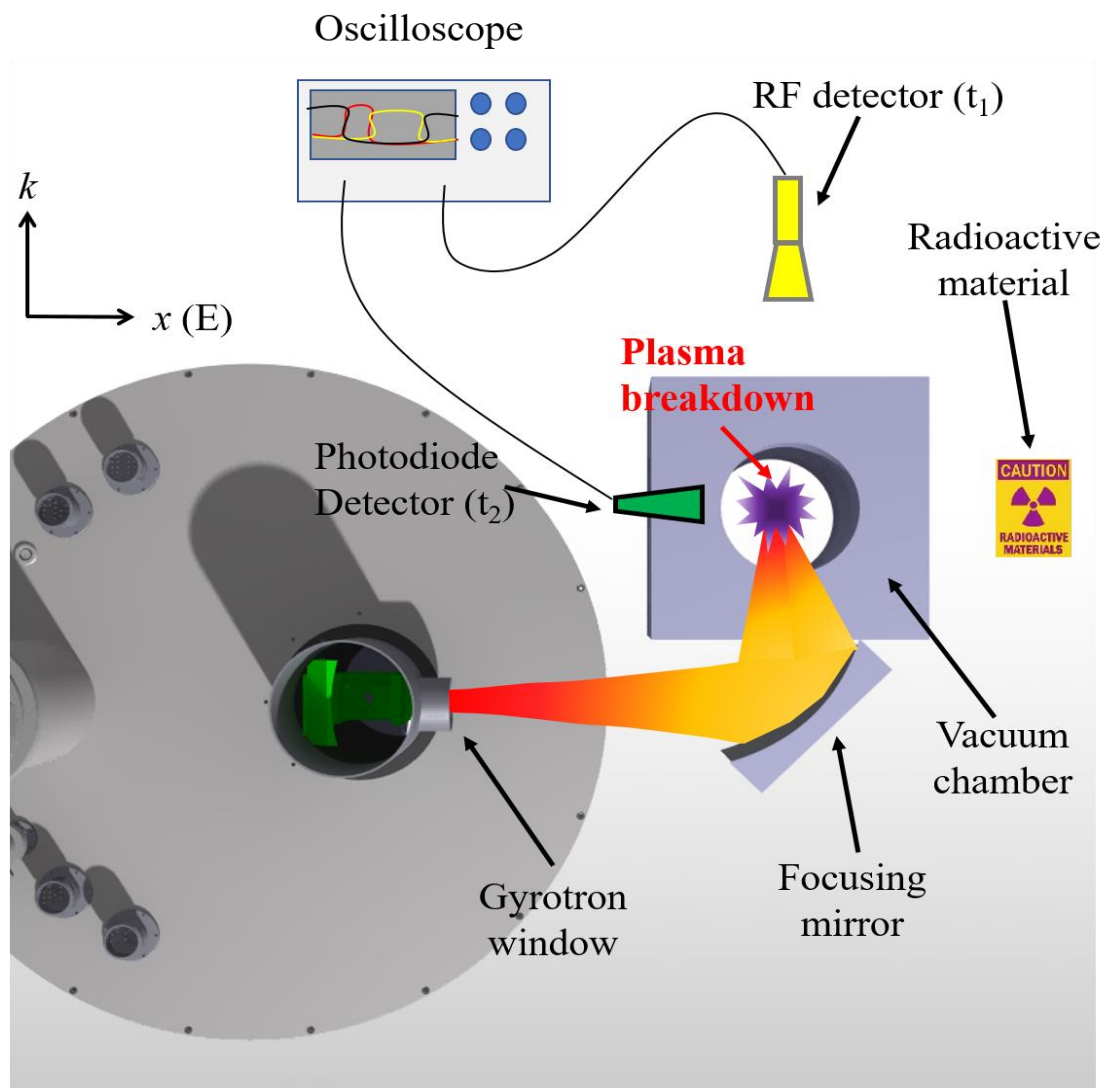


Figure 3-10: Experimental setup for the measurement of plasma discharge delay time with radioactive material.

The delay time was introduced in Section 2.2 and should be well-defined to analyze the results. The incident millimeter-wave passes through the vacuum chamber and is measured by the RF detector which indicates the onset time of the RF beam, t_1 . The t_2 is determined that RF wave signal rapidly decreases after the creation of the plasma discharge. This points out that the millimeter-wave is absorbed or reflected by plasma formation since the generated plasma acts like a conductor. There is also the photodiode detector to measure the fluorescent light caused by the plasma same as the t_2 . Thus, the time interval between the t_1 and t_2 signal is defined as total delay time with a precision of less than $0.1 \mu\text{s}$.

Chapter 4

Results of Plasma Breakdown for Radioactive Material

4.1 Experimental results for Ar plasma breakdown

4.1.1 Plasma breakdown image

Figure 4-1 shows the plasma breakdown image using a Phantom V2512 with $1\mu\text{s}$ minimum shutter speed at 300 Torr. The sensor resolution is 1280×800 with 25,600 pps of the 1 Mpx sensor. The camera lens is about 30 cm to the right side of the chamber. At 300 Torr, the incident power was near the threshold value without 100% occurrence for initiating plasma breakdown to prevent the plasma formation from diffusing. The plasma was generated $1.89\mu\text{s}$ later with $7.14\mu\text{s}$ of exposure time shown in Fig. 4-1(b). The observed filament array was called “fish bone” structure and was about 1.04 mm which had small discrepancy of the known parameter, $\lambda/4$ ($=0.79\text{ mm}$) due to the diffusing of the plasma and resolution of the camera.

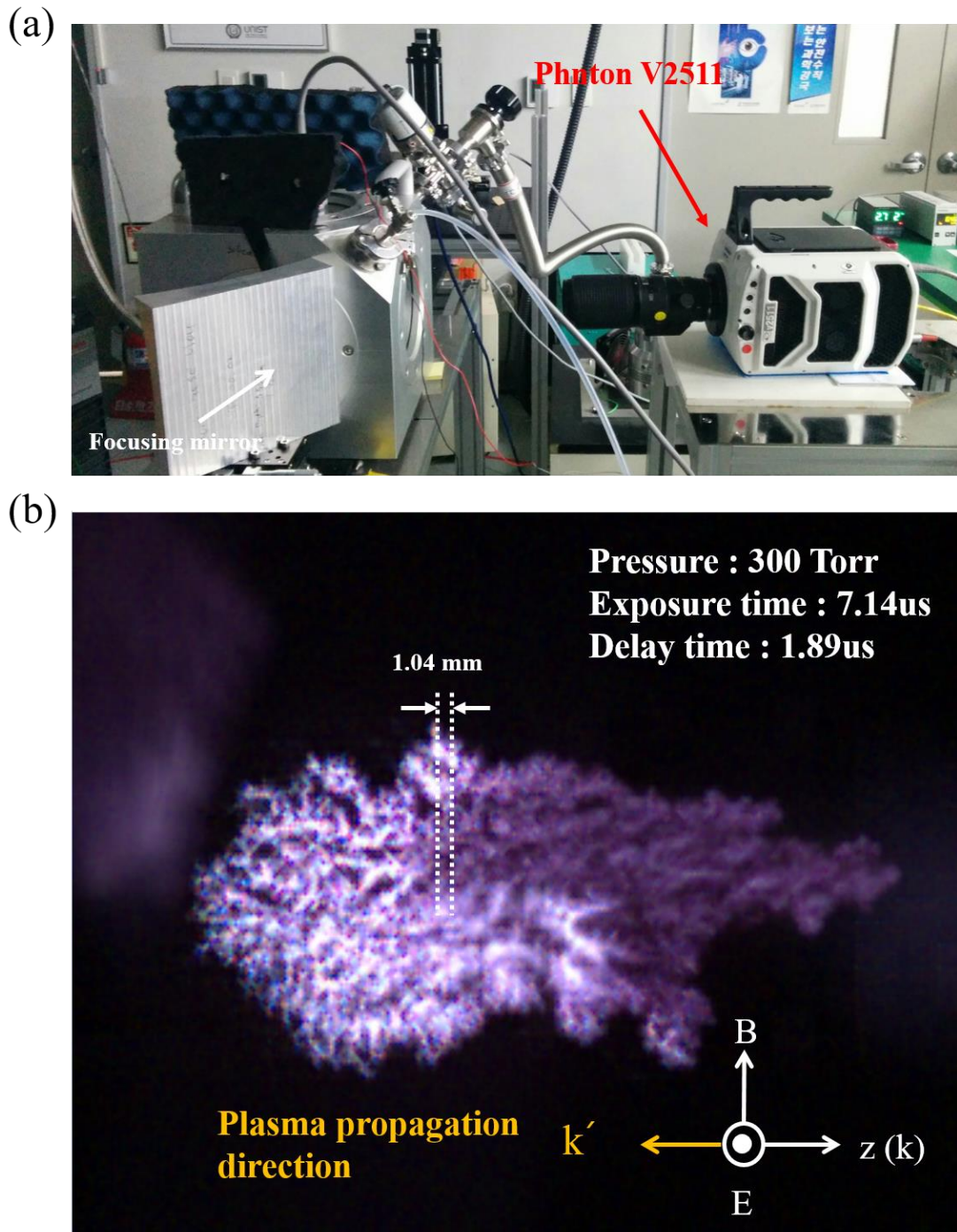


Figure 4-1: Plasma image measurement for the measurement of plasma discharge delay time. (a) The fast camera is located on the right side of the chamber. (b) The EM wave propagates in $z(k)$ direction. However, the plasma propagates in k' direction opposite direction of the incident wave because the plasma performed like a conductor and intensity of the beam was high along the opposite direction after plasma occurs at focal point.

4.1.2 Plasma velocity

The measurement of the plasma velocity was performed in the threshold electric field of 100 Torr with Ar gas using an intensified charge-coupled device (ICCD), model Andor iStar 320T Gen3 18F-63. As displayed in Fig 4-2(a), the ICCD camera is placed in a vertical direction to capture the electric field image. Figure 4-2(b) illustrates a movement of the plasma to evaluate the velocity of the plasma. The initial image was captured for an exposure time of $0.4 \mu\text{s}$ in each measurement. The second image was allowed after $0.4 \mu\text{s}$ of the creation of the plasma formation, and the peak intensity of the plasma moved 0.66 cm . From this movement of plasma image, the velocity of the plasma was calculated as 16.75 km/s .

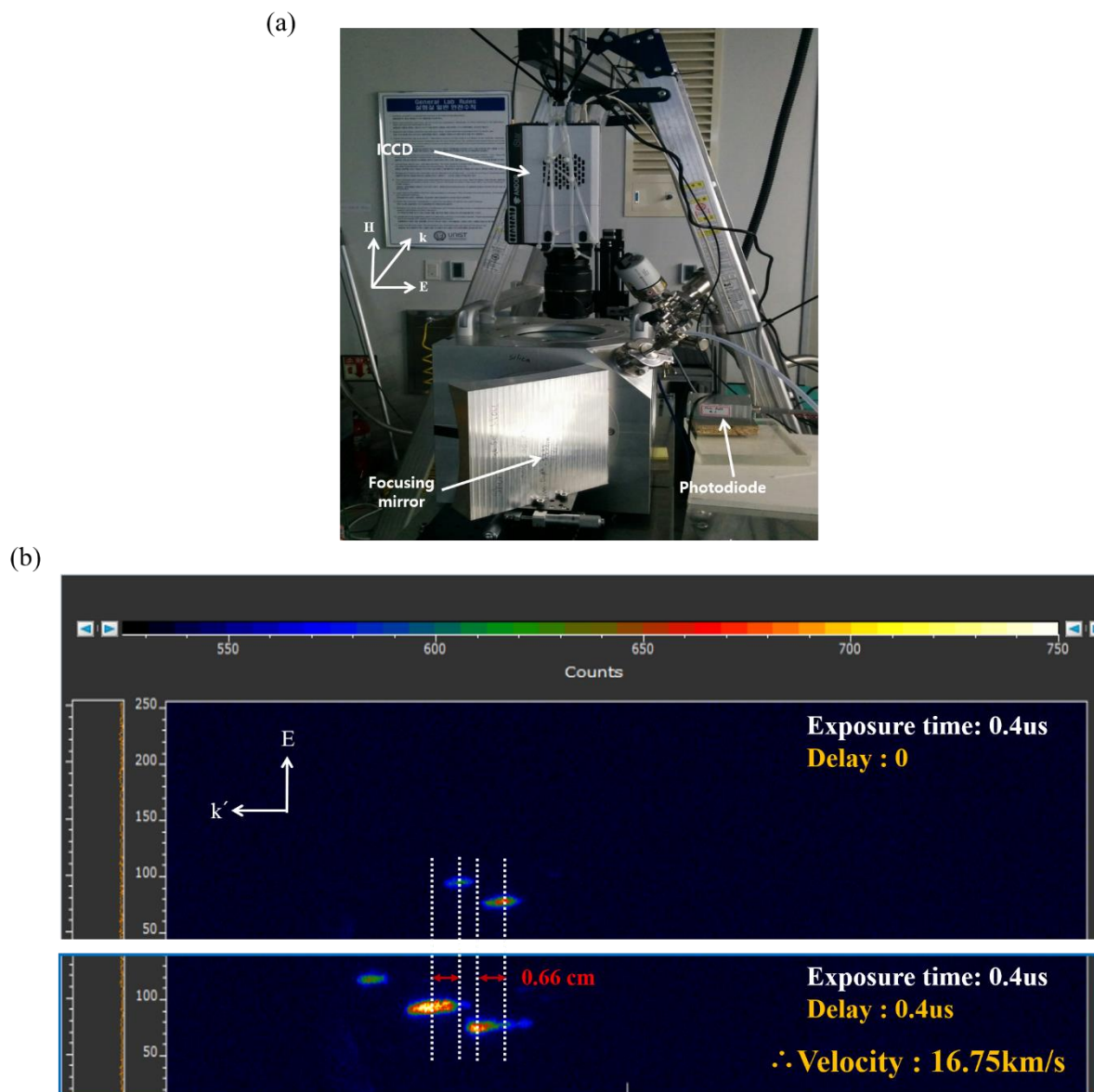
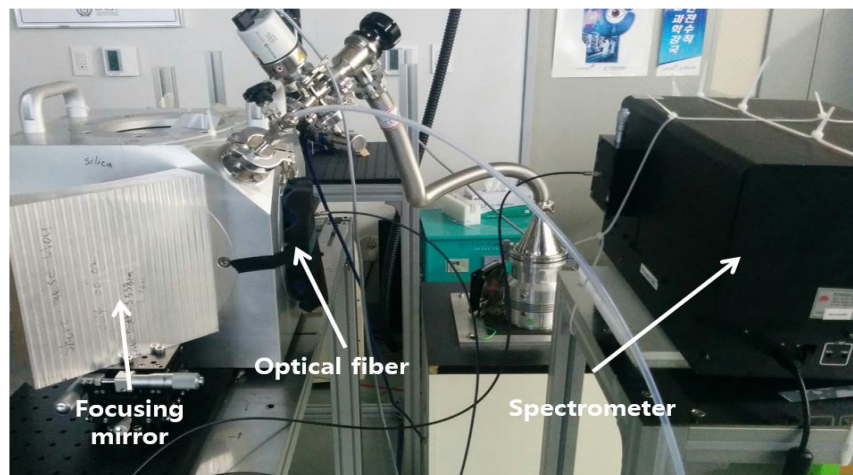


Figure 4-2: Plasma velocity measurement using the ICCD camera. (a) Experimental setup for the plasma velocity. (b) Movement of the plasma formation in different time interval.

4.1.3 Spectroscopy

A spectrum of the plasma breakdown was measured same condition of previous Section 4.1.2. The adopted device was Monora 320 spectrograph with an iDus Du420A CCD camera. The optical fiber is located on near the chamber window with measuring range from 200 nm to 1000 nm presented in Fig.4-3(a). The fluorescent light was collected for 1 s of the integration of the signal, and a background signal was eliminated as the reference data. The spectrum signal from the Fig. 4-3(b) indicates the amount of photons as a function of wavelength [26]. The measurement result of spectrum well coincides with the common Ar plasma emission spectrum.

(a)



(b)

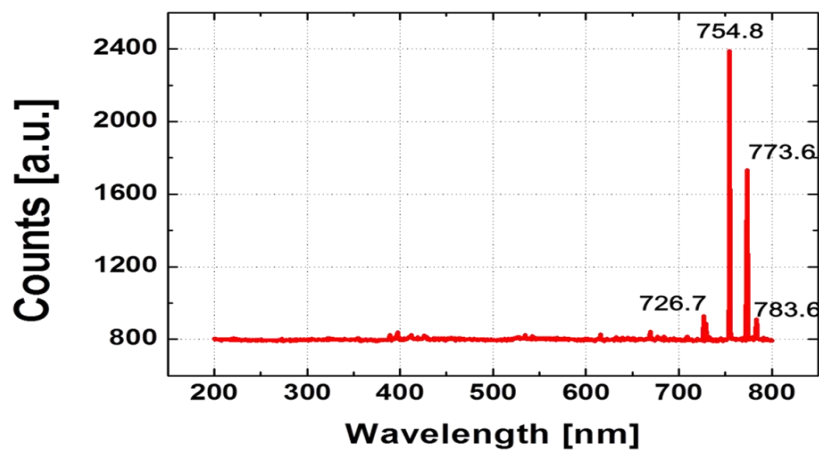


Figure 4-3: Spectroscopy measurement in Ar plasma using spectrometer. (a) Measurement setup for the Ar plasma. (b) Spectroscopy result shows that the spectrum signal induced by the fluorescent light is near 700 nm.

4.2 Experimental results for breakdown threshold electric field

To investigate the experimental data for Paschen curve, we initially performed the plasma breakdown experiment in various pressure range with Ar gas since the output power of our gyrotron is not enough to occur the plasma breakdown in atmospheric condition theoretically. After confirming that radioactive material reduced the required electric field for plasma initiation, the air experiment was conducted at 60 Torr and 760 Torr. The theoretical and experimental results revealed in Fig. 4-4 indicate the different required electric field for plasma discharge as a function of pressure [19], [27]. The experimental threshold electric field in each pressure shown in Fig. 4-4 was defined as the manifestation of 100% plasma volume breakdown with 20 μ s pulse duration of 1 Hz repetition over 200 shots. The required effective electric field was monitored for average value using the software LabVIEW ver. 2014. The variance of the introduced electric field had 0.15 kV/cm. Our maximum electric field induced by the millimeter-wave device was calculated as 3.49 kV/cm, equal to 32 kW of output power, green dotted line in Fig. 4-4. The red plus signs and blue crosses represent the experimental data in Ar condition with and without radioactive material case, respectively. The blue crosses represent that we cannot induce the breakdown discharge effect 100% over 250 Torr. Otherwise, with radioactive material (0.64 mCi of ^{60}Co) which is located at 20 cm from the concentration point of the incident wave, a visible light is emitted until 460 Torr. A reduction factor due to the radioactive source was about 1.7 which came from the generated secondary electron by Compton scattering of gamma photons and neutral Ar particle. As the pressure increased over 100 Torr, there is a discrepancy between the simulation results and experimental data. Interestingly, the attenuated RF signal was detected even at 760 Torr with Ar gas even though the theoretically required electric field at 760 Torr is about 15.7 kV/cm to initiate the breakdown. The photodiode and spectroscopic signal, however, could not detect the plasma owing to the extremely low photon intensity. In case of 60 Torr and 760 Torr air condition, the experiment was implemented as minimum pressure of Paschen curve and 1 atm case. Over 29 kW of the output power, we observed same phenomenon only with the field enhancing material, radioactivity (black circles in Fig. 4-4). In reference to this unusual occurrence, we named as under-threshold condition when the electron ionization avalanche was not completely achieved.

The experimental evidence of the under-threshold condition is presented in Fig. 4-5. Black and pink line indicate the RF signal in ambient condition and fully enhanced plasma discharge form. However, the 760 and 60 Torr in air and 760 Torr in Ar environments were not completely attenuated because of the inadequate output power. With the calibrated RF detector, we could estimate the plasma density based on the transmittance values measured during the experiment. The calculated plasma densities were $6.44 \times 10^{13} \text{ cm}^{-3}$ at 760 Torr in air, $6.23 \times 10^{13} \text{ cm}^{-3}$ at 760 Torr in Ar, and $5.87 \times 10^{13} \text{ cm}^{-3}$ at 60 Torr

in air shown in Table 4-1. These considered plasma densities did not reach the critical density, which was defined that the angular frequency was same with plasma frequency to occur the plasma avalanche ionization.

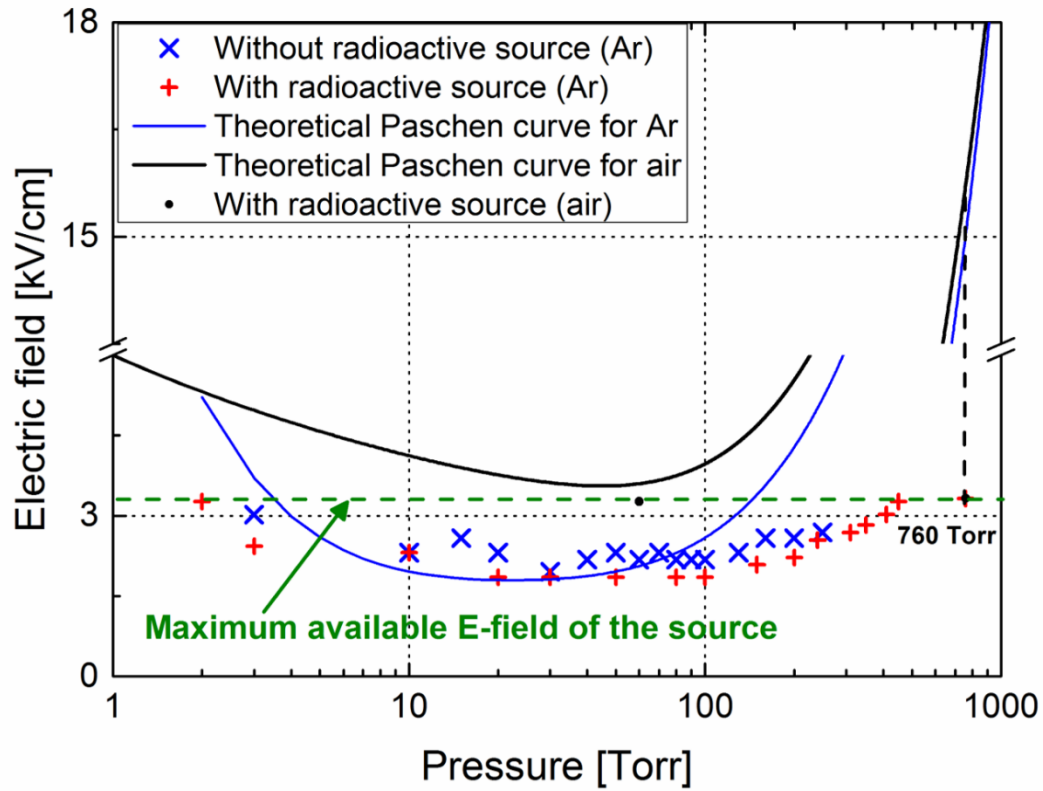


Figure 4-4: Theoretical Paschen curve and experimental measurement of threshold electric field for breakdown in Ar and air.

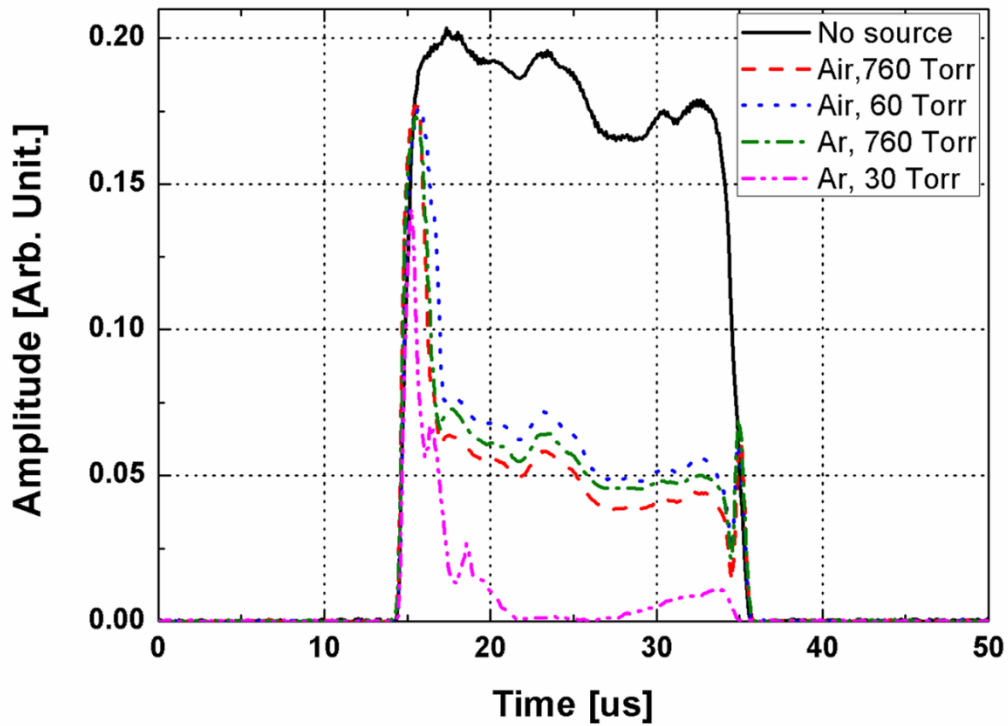


Figure 4-5: Amplitude of the RF signal under different pressure in Ar and air.

Table 4-1: Calculated plasma densities using the attenuated RF signal in different condition

Pressure (gas)	Transmittance	Plasma density
760 Torr (air)	0.19	$6.44 \times 10^{13} \text{ cm}^{-3}$
760 Torr (Ar)	0.20	$6.23 \times 10^{13} \text{ cm}^{-3}$
60 Torr (air)	0.22	$5.87 \times 10^{13} \text{ cm}^{-3}$

4.3 Experimental results for delay time

4.3.1 Delay time in Ar condition

Analysis of latency for plasma breakdown is another tremendous proof of the existence of radioactive material. The formative delay time and statistical delay time were defined and derived in previous Section 2.2, and the experimental data with and without source as a function of delay time were

displayed in Fig. 4-6 [28]. The source generation term $S=6 \mu\text{s}^{-1}$ in equation (2.27) was empirically selected on the background ionization rate owing to gamma photons. The plasma breakdown with an emission of the light was conducted up to 250 Torr without external source, and the data were plotted with and without case. The probability of no breakdown described in Fig. 4-6 points out that the plasma breakdown does not follow until 2.88 μs of pulse length at 30 Torr (blue circles). In other words, the minimum delay time over 200 samples in normal condition is 2.88 μs , and the collective data are listed in ascending order. From this analysis, we easily identified the distribution of delay time in various pressure. Owing to the existence of radioactive source, both formative delay time and statistical delay time were decreased in all pressure. These typical appearances make it possible to confirm the presence of the emissive material.

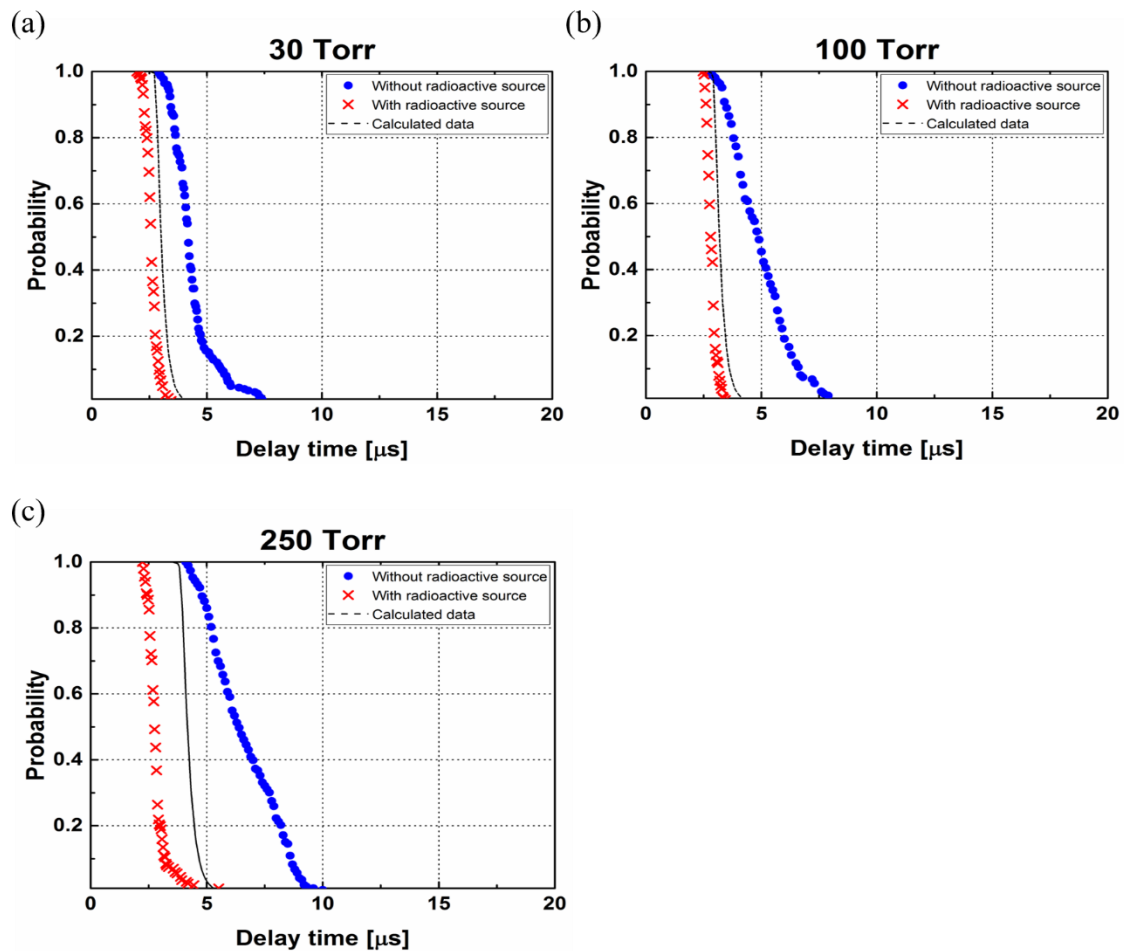


Figure 4-6: Survival rate for an incident RF wave during pulse duration. The experimental data are shown without radioactive material (blue circles) and with radioactive material (red crosses). The black dotted line indicates the fit curve for the presence of radioactive material case using equation (2.28) [28].

Moreover, we investigate the possibility for detection of radioactive material in real-time measurement. As shown in Fig. 3-9(b), there is an auto-controlled gate in front of lead chamber. Inner pressure was 250 Torr and the output power was fixed at 19 kW. The initial distance was 20 cm between incident beam waist position and radioactive material, and the remotely controllable gate opened and closed every 30 second to distinguish the existence of radioactivity. The combined data were simplified from the minimum delay time to 50% of the total amount of sample. As plotted in Fig 4-7, the experimental results operating the W-band gyrotron demonstrate the possibility in real situations. The delay time distribution without source (blue circles) is greatly wider than with condition (red squares). We strongly say that delay time measurement is possible in real time.

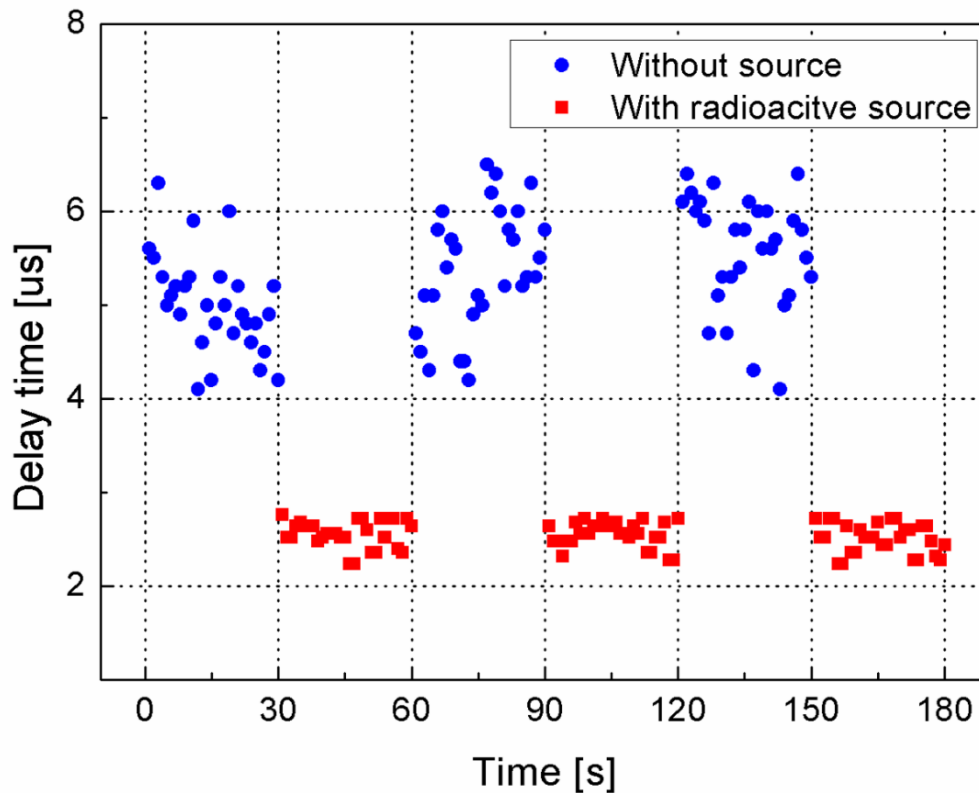


Figure 4-7: Real time measurement of delay time with and without radioactive material. The gyrotron operates at 19 kW and 250 Torr. The lead gate was opened and closed every 30 seconds to appear the radiation of ^{60}Co . The minimum delay time in each circumstance were 2.2 μs and 4.1 μs .

We looked at how delay time changes as the distance increases. The operation of the gyrotron oscillator was at 19 kW and 250 Torr, same as previous experiment. A meaning of the increase distance implies the reduction of the number of free electrons. This is an important constraint in order to ensure the distance of the detection range. The distance was initially 20 cm from the ^{60}Co source and gradually

increased up to 120 cm which was limitation of laboratory space. Figure 4-8 illustrates that the area of the delay time distribution increased following the distance increased. Even though most of the delay time distribution area were overlapped at 120 cm we could still differentiate the delay time dispersion due to the presence of radioactive material.

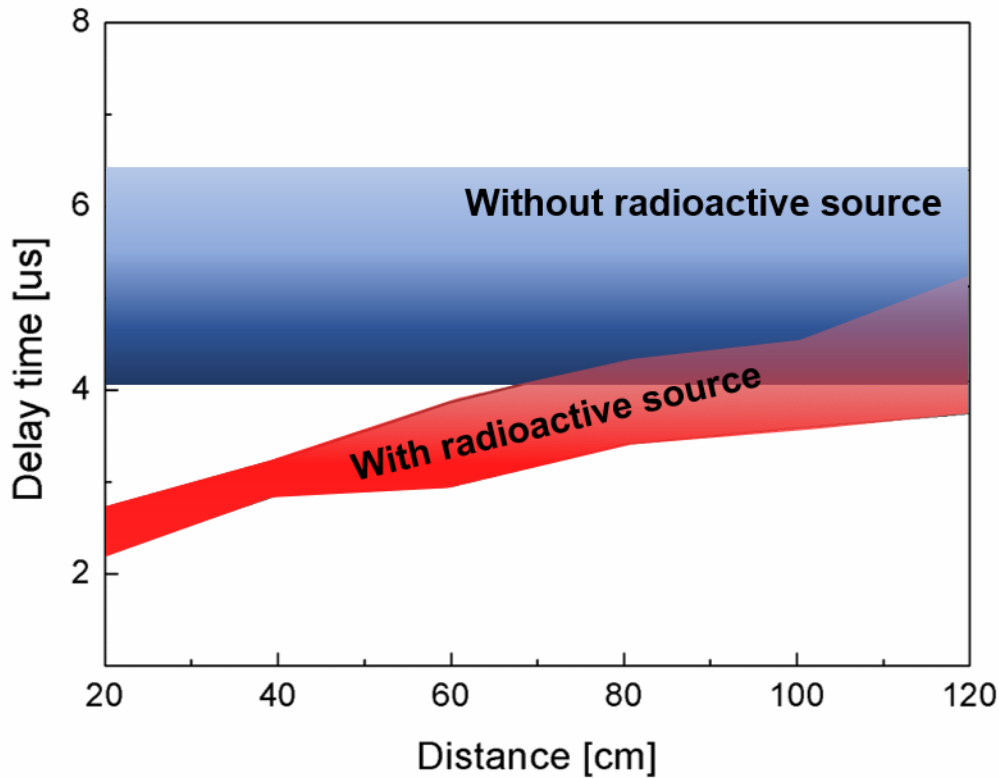


Figure 4-8: Real time measurement of delay time with and without radioactive material. As the distance increases from 20 cm to 120 cm, the dispersion of the delay time also spreads further.

The increased delay time as the distance growth is a close affinity with the average number of free electrons. The number of free electrons is calculated from 20 cm to examine the tendency of decreased free electrons. The operation condition of gyrotron was 28 kW, and inner pressure was 400 Torr in Ar gas which the plasma breakdown did not observed without radioactive source. As shown in Fig. 4-9, the probability of breakdown and the average number of free electrons using Monte Carlo N-Particle eXtended (MCNPX ver. 2.50) code were depicted as a function of distance [28]. As estimated, the probability for breakdown discharge decreased along the reduction of the amount of free electrons. At 270 cm from the 0.64 mCi of ^{60}Co source, the quantity of average free electrons eventually goes to 1 cm^3 .

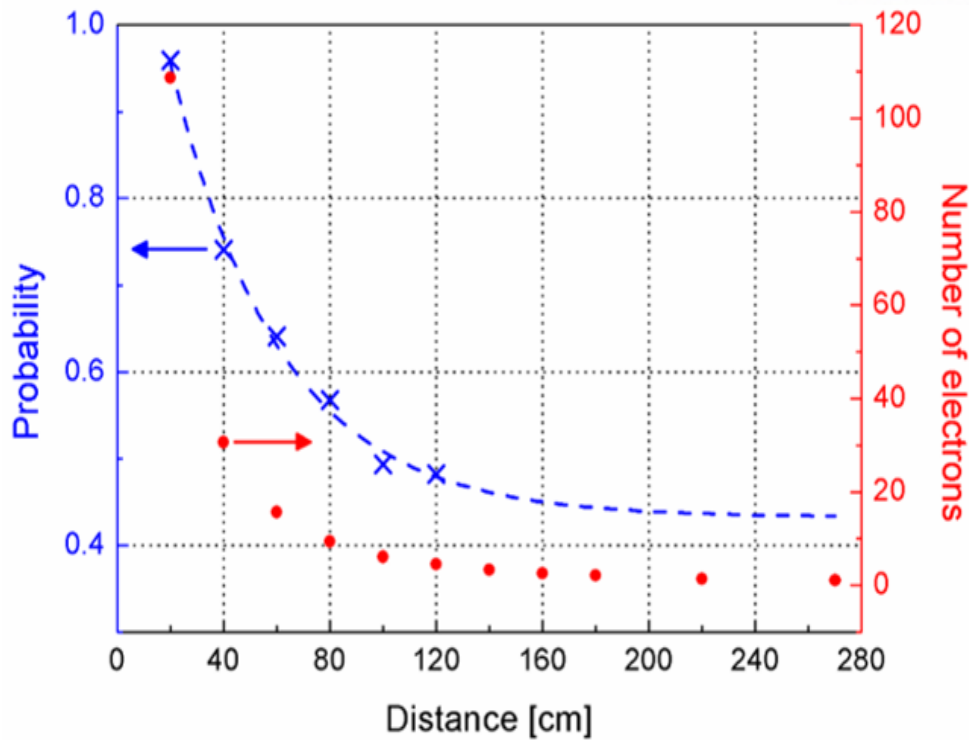


Figure 4-9: The probability of plasma breakdown and average number of free electrons using MCNPX code. This experiment is performed at 28 kW in 400 Torr of Ar gas. The experimental result of probability decreases exponentially with increasing distance. The reason of reduction is owing to the decrease of the average number of free electrons [28].

The under-threshold condition is evaluated in Ar at 760 Torr. The inconstant parameter is only incident RF power to investigate the delay time variations. As shown in Fig. 4-10(a), the distribution of delay time in both 30 kW and 32 kW are narrow, and the starting location of the formative delay time for 32 kW is shorter than 30 kW. The higher output power easily induces the plasma breakdown even in under-threshold condition. The delay time distribution in different incident power is shown in Fig. 4-10(b). The breakdown phenomenon was observed only with the radioactive source, and the attenuated RF signal was disappeared after elimination of the radioactivity. Same tendency with light emission of plasma breakdown, the higher output power of microwave beam decreases the delay time at fixed pressure. It is almost impossible to distinguish the amplitude of various output power at 30 Torr in Ar, because the enough power provides the narrow width of delay time dispersion. At 760 Torr in Ar case, the delay time becomes shorter as the power increased from 29 kW to 32 kW.

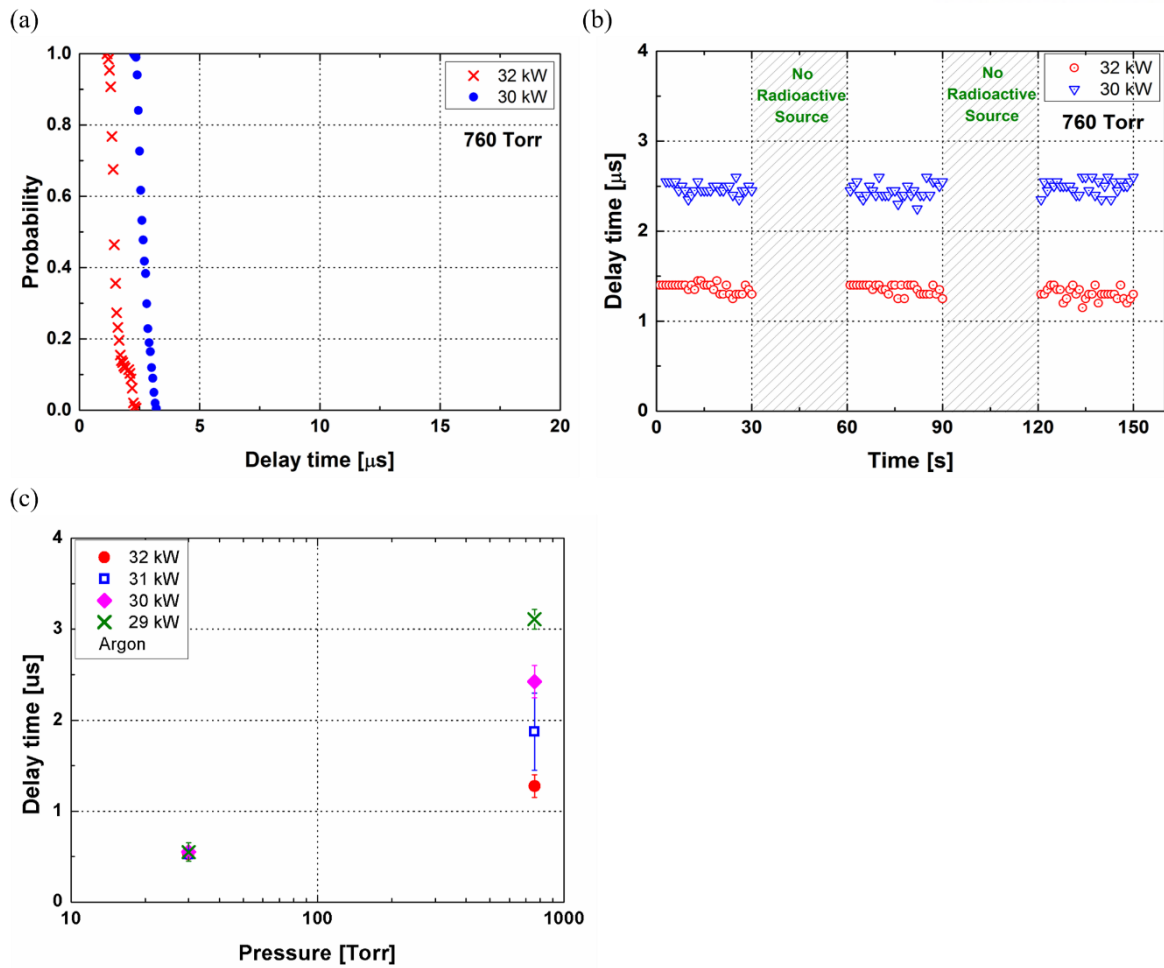


Figure 4-10: The experimental results in under-threshold condition. (a) Total probability for breakdown discharge as a function of time. (b) Delay time distribution with and without source at 30 and 32 kW. (c) Delay time distribution in different output power at 30 and 760 Torr [28].

4.3.2 Delay time in air condition

The air breakdown was performed around 30 kW at 60 and 760 Torr. In case of 60 Torr, the required threshold electric field is 3.56 kV/cm, which is over the maximum electric field of the introduced our gyrotron to initiate the breakdown avalanche ionization, and much higher amplitude of the electric field is essential in the atmospheric air condition shown in Fig. 4-4 so that the breakdown does happen only with the radioactive material. However, the reduced RF pulse was observed at 60 and 760 Torr in the air situation same as 760 Torr in Ar gas (see Fig. 4-5). From the Fig. 4-11, we intensely insist that this phenomenon is a reliable confirmation for detection of radioactive material. The results of (a) and (b) in Fig. 11 point out the probability of no breakdown in different incident power at 60 and 760 Torr. The real-time measurement in air condition is shown in Fig. 4-11(c) and (d). Just as we expected, the plasma

breakdown was initiated by the radioactive source, from 0 to 30 second. Higher output power ramped down the delay time at fixed pressure. However, the RF pulse was not saturated without radioactive source, from 30 to 60 seconds. As the pressure increased from 60 to 760 Torr, the delay time increased similar to the Ar experiment (see Fig. 4-11(e)) [28].

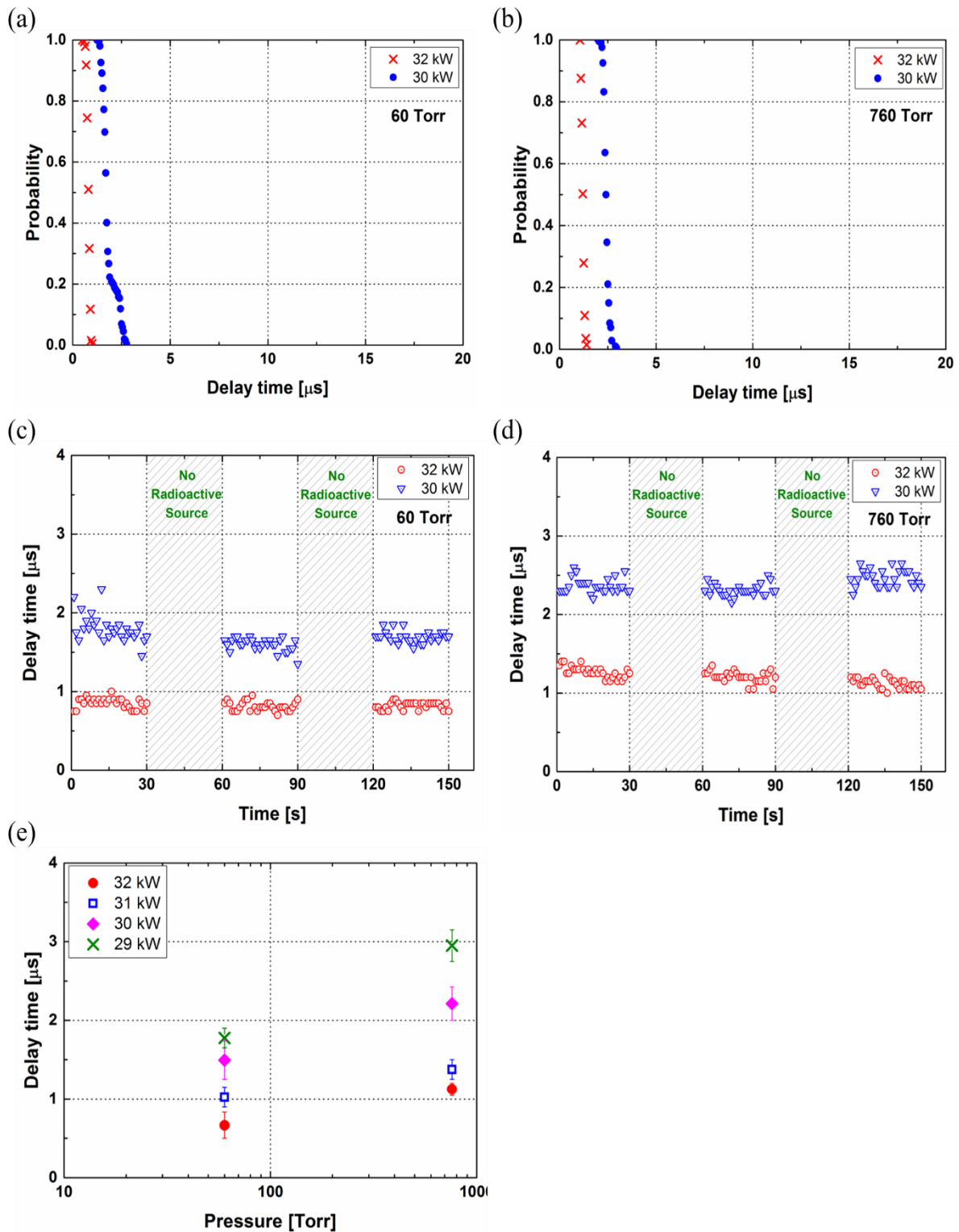


Figure 4-11: The experimental results in under-threshold condition in air. (a) & (b) Total probability for breakdown discharge as a function of delay time. (c) & (d) Delay time distribution with radioactive source at 30 and 32 kW. The hatched areas show the ambient condition so that plasma breakdown does not occur. (e) Delay time distribution in various output power at 60 and 760 Torr [28].

4.4 Analysis of delay time measurement

4.4.1 Sensitivity of Delay time

In this section, we discuss a detection method comparing our delay time method and detectable mass equation which is introduced by University of Maryland [13]. The detectable mass equation is based on the fact that, the existence of free electrons in breakdown-prone volume determines the concealed radioactive material. Naturally, there is no electron inside of the breakdown-prone volume, which means that the volume size is small enough so that the occurrence of plasma breakdown implies the existence of field enhancing source in the vicinity of this volume. The size of the beam in a focal plane can be expressed as [11]

$$\rho_0 = \frac{1}{\sqrt{\pi}} \cdot \frac{L}{R} \lambda, \quad (4.1)$$

where L is for the distance from an antenna to the focal point of the beam, R is the radius of the antenna, and λ is the wavelength of the RF beam. In our experiment, ρ_0 was 0.32 cm. From this value, we finally obtained the breakdown-prone volume using [11]

$$V = \frac{\pi^2}{3} \cdot \frac{\rho_0^4}{\lambda} \left\{ \frac{2}{3} \left(5 + \hat{P} \right) \sqrt{\hat{P}-1} - 4 \arctan \left(\sqrt{\hat{P}-1} \right) \right\}, \quad (4.2)$$

where $\hat{P} = P / P_{th}$ is the ratio of the wave power to its threshold value in the focal plane. For $\hat{P} = 2$, the breakdown-prone volume in our experimental case was calculated to be 0.17 cm³.

And then, the detectable mass equation is written as

$$M(g) \geq \frac{4\pi L_{\gamma,a} d^2}{AV\tau_{pulse}} \frac{\Delta E}{\langle E \rangle} \frac{v_i}{v_{i,eff}} \exp(d / L_{\gamma}), \quad (4.3)$$

where $L_{\gamma,a} = 1/n_a\sigma_a$ ($=280$ m, n_a is the density of air) is the propagation distance of gamma ray and is decided by the average absorption cross-section, σ_a which is responsible for the production of free electrons. The distance (d) is from the source to focal point; A is the specific activity, which is 1.1×10^3 Ci/g for ⁶⁰Co; the breakdown-prone volume $V = 0.17$ cm³ calculated in equation (4.2). τ_{pulses} is the pulse

duration (s); $\frac{\Delta E}{\langle E \rangle}$ is the ratio of the energy required to produce one secondary electron-ion pair to that of the primary electrons generated by the gamma rays; $\frac{V_i}{V_{i,eff}}$ is the ratio of the ionization frequency to the net ionization frequency; and $L_\gamma = 1/n_a \sigma_T (=130 \text{ m})$ is the gamma ray propagation distance and is determined by the total interaction cross-section, σ_T , owing to the Compton scattering in air. When the distances (d) are 20 and 120 cm, the calculated detectable mass is confirmed to be 0.067 mg and 2.4 mg respectively. At 20 cm, the experimentally determined detectable mass indicates a sensitivity roughly 130 times greater than that predicted by the theoretical estimation (equation 4.2), because the amount of 0.64 mCi of ^{60}Co used in our experiment is converted to 0.5 μg of pure ^{60}Co . At 120 cm, the proposed our method becomes 4800 times more sensitive than theoretically predicted. The theoretical estimation is based on the plasma on/off phenomenon, and our suggestion is measurement of plasma breakdown delay time which can reduce the frequency regime.

4.4.2 Reduction of required electric field with radioactive material

We deliberate how the detection of radioactive material in atmospheric air and Ar condition is possible with insufficient electric field for avalanche ionization. Breakdown occurs when the electron density reaches the critical density written as

$$n_{cr} = \frac{\omega^2 m \epsilon_0}{e^2} \quad (4.4)$$

Therefore, the delay time for the occurrence of breakdown is obtained under the condition

$$n_{cr} \leq n_0 e^{V_{eff,i} \cdot \tau} \quad (4.5)$$

$$\text{or, } V_{eff,i} \geq \frac{1}{\tau} \ln \left(\frac{n_{cr}}{n_0} \right). \quad (4.6)$$

The effective ionization frequency, $V_{eff,i}$, is a function of the amplitude of the RF field, E_0 , therefore, one can express for the ionization rate as

$$\nu_{\text{eff},i}(E_0) = \nu_{\text{am}} Y \left(\frac{E_0}{E_{\text{cr}}} \right), \quad (4.7)$$

where E_{cr} is the critical electric field for inducing breakdown, and ν_{am} is the typical dissociative attachment frequency. For $E_0 = E_{\text{cr}}$, $Y(1) = 1$, which means that the ionization rate is equal to the attachment rate to the molecules [29]. When the applied E_0 is considerably greater than the critical electric field, the ionization frequency is higher than the attachment frequency. This induces plasma breakdown.

From equation (4.7), the inverse function of Y is given by

$$Y \left(\frac{E_0}{E_{\text{cr}}} \right) = \left(\frac{\nu_{\text{eff},i}(E_0)}{\nu_{\text{am}}} \right), \quad (4.8)$$

$$\frac{E_0}{E_{\text{cr}}} = Y^{-1} \left(\frac{\nu_{\text{eff},i}(E_0)}{\nu_{\text{am}}} \right). \quad (4.9)$$

Substituting (4.6) into (4.9), and manipulation in terms of Y , and then

$$Y = \frac{1}{\tau_p \nu_{\text{am}}} \ln \left(\frac{n_{\text{cr}}}{n_0} \right). \quad (4.10)$$

Hence, if the incident RF field is same as the threshold field, and the ratio of the threshold field to the critical field is given by

$$\frac{E_0}{E_{\text{cr}}} \propto \frac{1}{\tau_p \nu_{\text{am}}} \ln \left(\frac{n_{\text{cr}}}{n_0} \right). \quad (4.11)$$

Therefore, the threshold field (E_0) is inversely proportional to the pulse length (τ_p), which indicates the longer RF pulse results in a decrease in the threshold field amplitude for plasma breakdown [27]. Furthermore, E_0 depends on the logarithm of the ratio of the critical plasma density to the number density of the initial seed electrons.

The equation (4.11) provides a reduction factor between E_0 and E_{cr} owing to a field enhancing material. We make a postulate that the increased conductivity in the breakdown-prone volume leads to the

reduction of the electric field amplitude for plasma breakdown. Thus, the field reduction factor, β , for decreased electric field is given by

$$\beta E_0 = E_{cr}, \quad (4.12)$$

where $\frac{1}{\beta} = \ln\left(\frac{n_{cr}}{n_0}\right) / \ln\left(\frac{n_{cr}}{n_0^*}\right) = \ln\left(\frac{n_0^*}{n_0}\right)$. Here, n_0 is the initial electron density without any external source (around $1\sim 10$ /cm³ in normal condition), and n_0^* is the seed electron number density in the presence of radioactive material. The calculated number of free electrons generated by the high energy gamma photons are approximately 50, and they have the average energy of 0.44 MeV using MCNPX code displayed in Fig. 4-12. Consequently, the high energy of single electron reproduces a number of secondary knock-on electrons expressed by

$$\frac{0.44 \text{ MeV}}{34 \text{ eV}} = 12600. \quad (4.13)$$

The estimated collision time for a high energy electron with an air molecule can be written as

$$t_{coll} = \frac{l}{v} = 1.6 \times 10^{-9} \text{ s}, \quad (4.14)$$

where l is the mean free path for the high energy electron, and v is the velocity of the electron. The mean free path for the high energy electron can be calculated as

$$l = \frac{1}{\sigma n_{air}}, \quad (4.15)$$

where σ is the scattering cross-section of free electrons, and n_{air} is the air density. The scattering cross-section of 0.44 MeV energy electron is around 10^{-17} /cm² [30], and n_{air} is around 10^{19} particles/cm³ at T=300 K and 760 Torr. The mean free path for the electron of high energy is approximately 100 μ m, and the collision time is approximately 4×10^{-13} s. A required total time for the generation of 12600 secondary electrons is calculated as 5×10^{-9} s. In summary, 50 high energy electrons during the 1 μ s before initiating the plasma breakdown generate around 1.3×10^8 electrons/cm³ for the total secondary knock-on electrons. Thus, the calculated reduction factor is 2.5 for the generated electron density

1.3×10^8 electrons/cm³. The relationship between the reduction factor, β , and the free electron density is illustrated in Fig. 4-13.

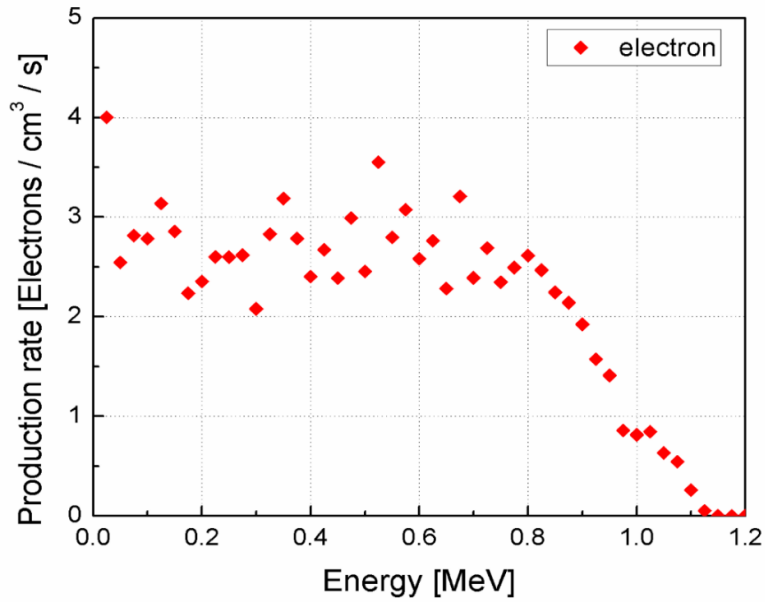


Figure 4-12: Production rate of electrons for 0.64 mCi of ⁶⁰Co located 20 cm away from center of the RF beam. The energy spectrum was calculated using MCNPX code.

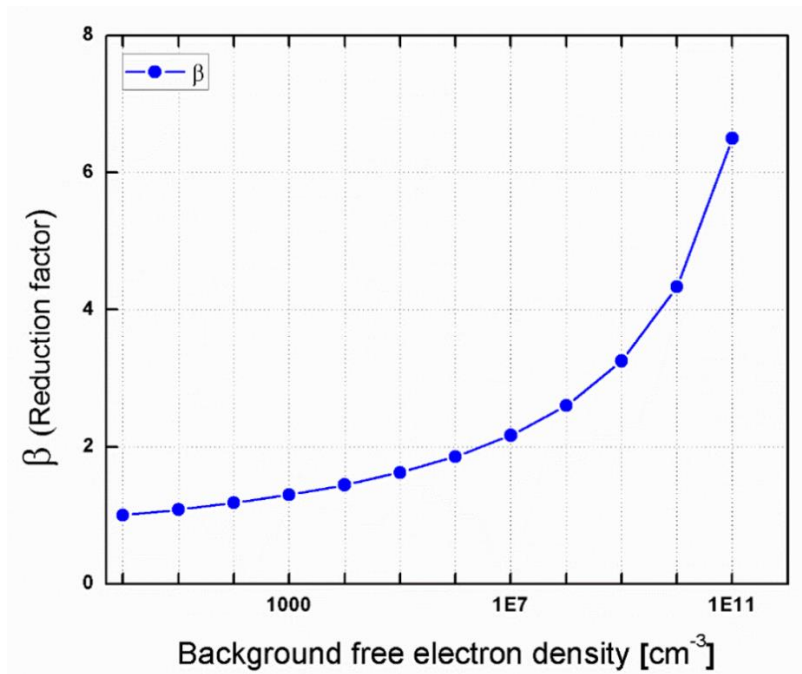


Figure 4-13: Electric field reduction factor (β) as a function of average free electron density.

4.4.3 Possible detection ranges and limitation

We introduce the detection range of current technology such as the Geiger-Muller counter. The radiation dose rate is given by

$$D(R/h) = \frac{\Gamma \times S}{d^2}, \quad (4.16)$$

where $\Gamma=1.32 \text{ R}\cdot\text{m}^2 / (\text{Ci}\cdot\text{h})$ is the specific gamma-ray constant for ^{60}Co , S is the radioactivity (Ci), and d (m) is the distance from the source to the GM counter. For example, the radiation dose rate of 0.64 mCi of pure ^{60}Co can be $1 \mu\text{Sv/h}$ ($R = 0.01$ Sieverts (Sv)), which is a dangerous level of the radiation exposure, at 2.5 m away from the source. However, the investigator should be in the vicinity of radioactive material and exposed to radiation.

Figure 4-14 represents the detection range in real world. Given the proper size of the antenna and wavelength of millimeter device, the detection distance is determined. The potential distance is expressed as $R(\text{m}) = 2D^2/\lambda$, where D and λ are the proper size of antenna diameter and the wavelength of the EM source.

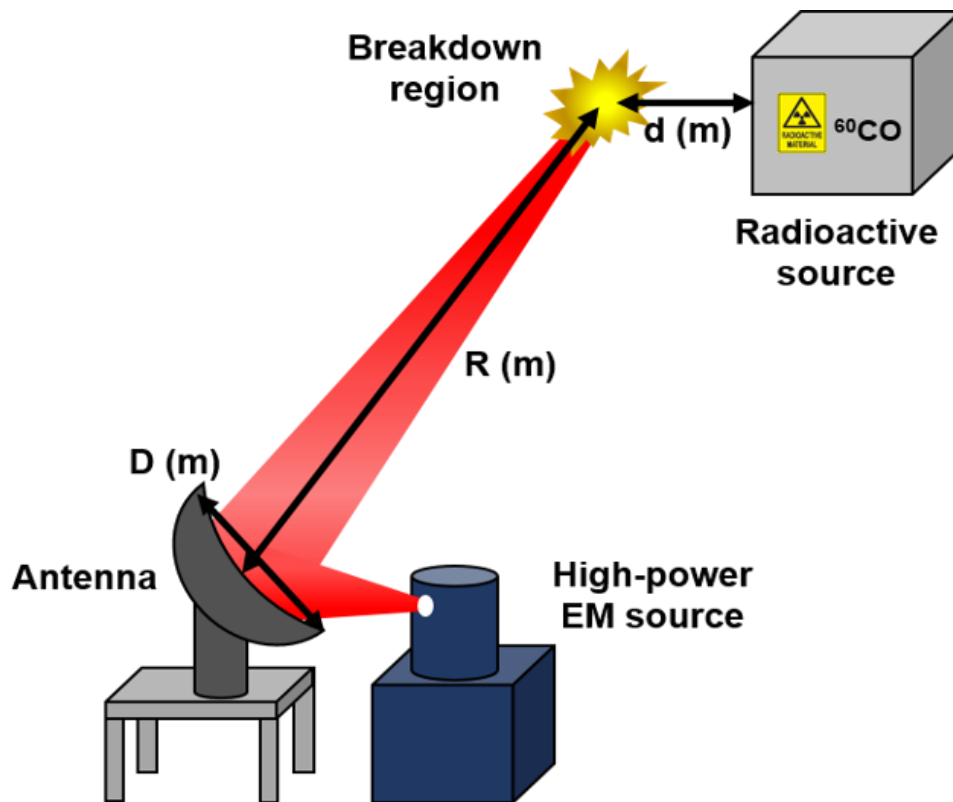


Figure 4-14: Possible detection ranges of radioactive material using high-power microwave source. The radioactive source is shielded in container.

Air turbulence is difficult to predict and impossible to eliminate in ambient air. Temperature and humidity changes cause the absorption coefficient of the millimeter/THz wave to change as well (although the effect is weaker than it is at optical frequencies), and pressure changes may occur over the course of a day. However, local and instantaneous air turbulence may be eliminated by averaging multiple shots of the incident EM wave pulses by increasing the repetition rate of the incident wave pulse. Let us consider the effect of beam wander on the detection range. For the weak turbulence case, the distance R (m) at which the turbulence is sufficiently weak to enable detection can be expressed as [31]

$$[R(\text{m})]^3 < \frac{10^{-2}[\rho_0(\text{m})]^2}{0.434C_n^2K}, \quad (4.17)$$

where ρ_0 is the beam width; C_n^2 is the strength of turbulent refractive-index irregularities and is between $3 \times 10^{-13} \text{ m}^{-2/3}$ and $6 \times 10^{-17} \text{ m}^{-2/3}$, which correspond to strong and weak turbulence, respectively. K is an integral coefficient ($\text{m}^{-1/3}$) defined as [31]

$$K = \int_0^\infty \frac{\exp(-\kappa^2 / v_m^2)}{(\kappa^2 + v_0^2)^{11/6}} \kappa^3 d\kappa, \quad (4.18)$$

where $v_0 = 2\pi/L_0$, and $v_m = 5.92/l_0$ are the wave numbers determined by the outer L_0 and inner l_0 scales of the turbulence, respectively. For our experimental setup, ρ_0 was around 5 mm and K is around 10~20 $\text{m}^{-1/3}$. Under these conditions, R varies from 50 m to 1 km depending on the strength of the turbulent parameter. Therefore, it is advantageous for the wavelength to be longer since R depends on the size of the focused incident EM beam. From this estimate, we can conclude that the remote detection range can be extended to ~50 m and that in an environment with low turbulence (or clear and calm weather), the remote detection range may be increased up to 1 km with an antenna size of 1 m and a 95 GHz source shown in Table 4-2.

Table 4-2: Comparable detection ranges in current technology and proposed method using delay time

	GM counter	95 GHz gyrotron
d (m)	~ 2.5	≥ 1.2
R (m)		50 (strong turbulence) 1000 (weak turbulence)

Chapter 5

Conclusion

This doctoral dissertation successfully demonstrated, for the first time, that it is possible to sense the concealed radioactive source using a high-power millimeter-wave oscillator, gyrotron. The theoretical delay time composed of the formative delay time and statistical delay time was derived to compare the experimental data. In addition, the underdense plasma density model was chosen to calculate for transmittance and reflectance of the attenuated RF wave signal. All components delivered in this experiment, including focusing mirror, vacuum chamber, RF detector, photodiode detector, and radioactive material were designed and fabricated to measure the plasma breakdown phenomenon as reported in Chapter 3. A fundamental study about Ar plasma breakdown was performed such a fish bone structure of the plasma filament array, the velocity of the plasma opposite to the RF wave, and the spectroscopy in Ar plasma.

A new finding of this study was the reduced required electric field with a presence of the radioactive material. This amplitude of the electric field was measured in pressurized Ar gas and atmospheric air condition. The theoretical reduction factor was 2.5 in our condition, and it was 4 from the experimental observation. There is a small discrepancy because of the uncontrollable experimental conditions containing calculation of the exact molecular composition and a humidity in experimental situations. Besides, the other reason was that the definition of the plasma volume breakdown was 100% occurrence of it during over 200 pulse shots with 1 Hz repetition. In the experiment, the lower threshold electric field was observed with insufficient plasma breakdown occurrence, less than 100%, but we did not take the electric field condition.

The sensitivity based on the delay time measurement was 4800 times higher than that predicted by theoretical approaches in terms of the detectable mass using plasma on/off phenomenon; this was achieved by measuring the plasma avalanche delay time with precision. The plasma on/off method is required high frequency of the output THz beam to make a small breakdown-prone volume without free electron in normal condition so that the created free electron by decaying of the radioactive material in

the breakdown-prone volume. On the contrary, the introduced proposal in thesis allows the lower frequency and output power owing to the reduction factor caused by radioactive material. If it is possible to develop the small size of the superconducting or permanent magnet for the gyrotron oscillator, the operating frequency can be decreased down to tens of GHz with the small size of the generator and the propagation distance will be increased up to hundreds of kilometers. The existing current technologies such as GM counters and ion chamber detectors can measure 1 $\mu\text{Sv/h}$ from the 0.64 mCi of ^{60}Co at 2.5 m away from the source. However, our proposed delay time analysis method allows to detect the radioactive material from 50 m with strong turbulence to about 1 km with weak turbulence shown in Table 4.2.

In summary, with analysis of reduced threshold electric field and delay time to initiate the plasma avalanche ionization, remote detection of radioactive material in long distance was possible using high-power millimeter-range gyrotron.

References

- [1] A. D. Macdonald, *Microwave Breakdown in Gases*. Wiley, New York, 1966.
- [2] Y. Hidaka, E. M. Choi, I. Mastovsky, M. A. Shapiro, J. R. Sirigiri, and R. J. Temkin, "Observation of large arrays of plasma filaments in air breakdown by 1.5-MW 110-GHz gyrotron pulses," *Phys. Rev. Lett.*, vol. 100, no. 3, pp. 3–6, 2008.
- [3] Y. Hidaka *et al.*, "Plasma structures observed in gas breakdown using a 1.5 MW, 110 GHz pulsed gyrotron," *Phys. Plasmas*, vol. 16, no. 5, pp. 1–7, 2009.
- [4] A. M. Cook, J. S. Hummelt, M. A. Shapiro, and R. J. Temkin, "Observation of plasma array dynamics in 110 GHz millimeter-wave air breakdown," *Phys. Plasmas*, vol. 18, no. 10, 2011.
- [5] A. Cook, M. Shapiro, R. Temkin, A. Cook, M. Shapiro, and R. Temkin, "Pressure dependence of plasma structure in microwave gas breakdown at 110 GHz Pressure dependence of plasma structure in microwave gas breakdown at 110 GHz," vol. 11504, no. 2010, pp. 2008–2011, 2013.
- [6] D. Dorozhkina *et al.*, "Investigations of time delays in microwave breakdown initiation," *Phys. Plasmas*, vol. 13, no. 1, pp. 1–7, 2006.
- [7] H. C. Kim and J. P. Verboncoeur, "Time-dependent physics of a single-surface multipactor discharge," *Phys. Plasmas*, vol. 12, no. 12, pp. 1–7, 2005.
- [8] P. J. Ford, S. R. Beeson, H. G. Krompholz, and A. A. Neuber, "A finite-difference time-domain simulation of high power microwave generated plasma at atmospheric pressures," *Phys. Plasmas*, vol. 19, no. 7, 2012.
- [9] C. J. Edgcombe, *Gyrotron Oscillators*. Taylor & Francis, 1993.
- [10] "<https://www.britannica.com/technology/gyrotron>."
- [11] G. S. Nusinovich *et al.*, "Development of THz-range gyrotrons for detection of concealed radioactive materials," *J. Infrared, Millimeter, Terahertz Waves*, vol. 32, no. 3, pp. 380–402, 2011.
- [12] G. S. Nusinovich, P. Sprangle, V. L. Granatstein, G. S. Nusinovich, P. Sprangle, and V. L. Granatstein, "Range , resolution and power of THz systems for remote detection of concealed radioactive materials Range , resolution and power of THz systems for remote detection of concealed radioactive materials," vol. 83303, 2011.
- [13] G. S. Nusinovich, P. Sprangle, V. E. Semenov, D. S. Dorozhkina, and M. Y. Glyavin, "On the sensitivity of terahertz gyrotron based systems for remote detection of concealed radioactive materials," *J. Appl. Phys.*, vol. 111, no. 12, 2012.
- [14] V. L. Granatstein, G. S. Nusinovich, V. L. Granatstein, and G. S. Nusinovich, "Detecting excess ionizing radiation by electromagnetic breakdown of air Detecting excess ionizing radiation by electromagnetic breakdown of air," vol. 63304, no. May, pp. 1–6, 2014.
- [15] J. T. Krile and A. A. Neuber, "Modeling statistical variations in high power microwave breakdown," *Appl. Phys. Lett.*, vol. 98, no. 21, pp. 2009–2012, 2011.
- [16] J. Foster, H. Krompholz, and A. Neuber, "Investigation of the delay time distribution of high power microwave surface flashover," *Phys. Plasmas*, vol. 18, no. 1, pp. 8–13, 2011.
- [17] M. Born and E. Wolf, *Principles of optics: electromagnetic theory of propagation, interference and diffraction of light*. 1980.
- [18] A. M. Cook, J. S. Hummelt, M. A. Shapiro, and R. J. Temkin, "Measurements of electron avalanche formation time in W-band microwave air breakdown," *Phys. Plasmas*, vol. 18, no. 8, 2011.
- [19] Y. P. Raizer and J. E. Allen, *Gas Discharge Physics*, 2nd ed. Berlin, Springer, 1997.
- [20] R. A. Wijsman, "Breakdown Probability of a Low Pressure Gas Discharge," *Phys. Rev.*, vol. 75, no. 5, pp. 833–838, 1949.
- [21] J. Foster, S. Beeson, M. Thomas, J. Krile, H. Krompholz, and A. Neuber, "Rapid formation of dielectric surface flashover due to pulsed high power microwave excitation," *IEEE Trans. Dielectr. Electr. Insul.*, vol. 18, no. 4, pp. 964–970, 2011.
- [22] L. Research, "Surf3d 2.43."

- [23] “CRYSTRAN.” [Online]. Available: <https://www.crystran.co.uk/>.
- [24] M. V. Katikeyan, E. Borie, and M. Thumm, *Gyrotrons: high-power microwave and millimeter wave technology*. Springer Science & Business Media, 2013.
- [25] S. G. Kim *et al.*, “System Development and Performance Testing of a W-Band Gyrotron,” *J. Infrared, Millimeter, Terahertz Waves*, vol. 37, no. 3, pp. 209–229, 2016.
- [26] D. Kim, S. G. Kim, A. Sawant, D. Yu, M. Choe, and E. Choi, “Study on statistical breakdown delay time in argon gas using a W-band millimeter-wave gyrotron Study on statistical breakdown delay time in argon gas using a W-band millimeter-wave gyrotron,” vol. 43505, pp. 1–5, 2016.
- [27] L. Gould and L. W. Roberts, “Breakdown of air at microwave frequencies,” *J. Appl. Phys.*, vol. 27, no. 10, pp. 1162–1170, 1956.
- [28] D. Kim *et al.*, “Remote detection of radioactive material using high-power pulsed electromagnetic radiation,” *Nat. Commun.*, vol. 8, no. May, p. 15394, 2017.
- [29] A. Gurevich, N. Borisov, and G. Milikh, *Physics of Microwave Discharges: artificially ionized regions in 176 the atmosphere*. CRC Press, 1997.
- [30] A. V. Phelps, L. C. Pitchford, and L. C. Pitchford~, “Anisotropic scattering of electrons by N₂ and its effect on electron transport,” *Phys. Rev. A*, vol. 31, no. 5, pp. 2932–2949, 1985.
- [31] G. S. Nusinovich, F. Qiao, D. G. Kashyn, R. Pu, and L. S. Dolin, “Breakdown-prone volume in terahertz wave beams,” *J. Appl. Phys.*, vol. 113, no. 23, 2013.